

## Novel injectable adhesive hydrogel loaded with exosomes for holistic repair of hemophilic articular cartilage defect

Qinfeng Yang<sup>a,b,1</sup>, Guihua Liu<sup>c,1</sup>, Guanghao Chen<sup>d,1</sup>, Guo Chen<sup>a,1</sup>, Keyu Chen<sup>a</sup>, Lei Fan<sup>b</sup>, Yuesheng Tu<sup>a</sup>, Jialan Chen<sup>b</sup>, Zhanjun Shi<sup>b,\*\*\*\*</sup>, Chuan Chen<sup>e</sup>, Shubo Liu<sup>a</sup>, Geyang Deng<sup>a</sup>, Xiaoqian Deng<sup>f</sup>, Chunhan Sun<sup>c</sup>, Xiaoyang Li<sup>g,\*\*\*\*</sup>, Shuofei Yang<sup>h,\*\*\*</sup>, Shaowei Zheng<sup>i,j,\*\*</sup>, Bin Chen<sup>a,\*</sup>

<sup>a</sup> Division of Orthopaedics and Traumatology, Department of Orthopaedics, Nanfang Hospital, Southern Medical University, Guangzhou, Guangdong, 510515, China

<sup>b</sup> Division of Orthopaedic Surgery, Department of Orthopaedics, Nanfang Hospital, Southern Medical University, Guangzhou, Guangdong, 510515, China

<sup>c</sup> Institute of Orthopaedics, Huizhou Central People's Hospital, Huizhou, Guangdong, 516008, China

<sup>d</sup> Department of Orthopaedics, The Second Hospital of Jiaxing, The Second Affiliated Hospital of Jiaxing University, Jiaxing, Zhejiang, 314000, China

<sup>e</sup> Department of Obstetrics and Gynecology, Core Facility Center, The First Affiliated Hospital of USTC, Division of Life Sciences and Medicine, University of Science and Technology of China, Hefei, Anhui, 230001, China

<sup>f</sup> State Key Laboratory of Ophthalmology, Zhongshan Ophthalmic Center, Sun Yat-sen University, Guangdong Provincial Key Laboratory of Ophthalmology and Visual Science, Guangzhou, Guangdong, 510060, China

<sup>g</sup> Department of Vascular Surgery, The Quzhou Affiliated Hospital of Wenzhou Medical University, Quzhou People's Hospital, Quzhou, Zhejiang, 324000, China

<sup>h</sup> Department of Vascular Surgery, Renji Hospital, School of Medicine, Shanghai Jiaotong University, Shanghai, 200127, China

<sup>i</sup> Department of Sports Medicine and Rehabilitation, Peking University Shenzhen Hospital, Shenzhen, China

<sup>j</sup> State Key Laboratory of Quality Research in Chinese Medicines, Laboratory of Drug Discovery from Natural Resources and Industrialization, School of Pharmacy, Macau University of Science and Technology, Macau, 999078, China

### ARTICLE INFO

#### Keywords:

Hemophilic articular cartilage defect  
Adhesive hydrogel  
Exosomes  
Anti-inflammation  
Chondrogenesis

### ABSTRACT

Hemophilic articular cartilage damage presents a significant challenge for surgeons, characterized by recurrent intraarticular bleeding, a severe inflammatory microenvironment, and limited self-repair capability of cartilage tissue. Currently, there is a lack of tissue engineering-based integrated therapies that address both early hemostasis, anti-inflammation, and long-lasting chondrogenesis for hemophilic articular cartilage defects. Herein, we developed an adhesive hydrogel using oxidized chondroitin sulfate and gelatin, loaded with exosomes derived from bone marrow stem cells (BMSCs) (Hydrogel-Exos). This hydrogel demonstrated favorable injectability, self-healing, biocompatibility, biodegradability, swelling, frictional and mechanical properties, providing a comprehensive approach to treating hemophilic articular cartilage defects. The adhesive hydrogel, featuring dynamic Schiff base bonds and hydrogen bonds, exhibited excellent wet tissue adhesiveness and hemostatic properties. In a pig model, the hydrogel could be smoothly injected into the knee joint cartilage defect site and gelled *in situ* under fluid-irrigated arthroscopic conditions. Our *in vitro* and *in vivo* experiments confirmed that the sustained release of exosomes yielded anti-inflammatory effects by modulating macrophage M2 polarization through the NF- $\kappa$ B pathway. This immunoregulatory effect, coupled with the extracellular matrix components provided by the adhesive hydrogel, enhanced chondrogenesis, promoted the cartilage repair and joint function restoration after hemophilic articular cartilage defects. In conclusion, our results highlight the significant application potential of Hydrogel-Exos for early hemostasis, immunoregulation, and long-term chondrogenesis in

Peer review under responsibility of KeAi Communications Co., Ltd.

\* Corresponding authors.

\*\* Corresponding authors.

\*\*\* Corresponding authors.

\*\*\*\* Corresponding authors.

\*\*\*\*\* Corresponding authors.

E-mail addresses: [18719096889@163.com](mailto:18719096889@163.com) (Z. Shi), [lixiaoyang1@wmu.edu.cn](mailto:lixiaoyang1@wmu.edu.cn) (X. Li), [doctor\\_yangshuofei@163.com](mailto:doctor_yangshuofei@163.com) (S. Yang), [zswljq@126.com](mailto:zswljq@126.com) (S. Zheng), [chb@smu.edu.cn](mailto:chb@smu.edu.cn) (B. Chen).

<sup>1</sup> These authors contributed equally to this work.

<https://doi.org/10.1016/j.bioactmat.2024.08.018>

Received 7 June 2024; Received in revised form 18 August 2024; Accepted 19 August 2024

2452-199X/© 2024 The Authors. Publishing services by Elsevier B.V. on behalf of KeAi Communications Co. Ltd. This is an open access article under the CC BY-NC-ND license (<http://creativecommons.org/licenses/by-nc-nd/4.0/>).

hemophilic patients with cartilage injuries. This innovative approach is well-suited for application during arthroscopic procedures, offering a promising solution for addressing the complex challenges associated with hemophilic articular cartilage damage.

## 1. Introduction

Articular cartilage defects are prevalent in orthopedic practice, affecting individuals across all age groups and resulting in pain, deformity, and disability, thereby imposing a substantial burden on healthcare systems [1–5]. Due to the absence of vascular, neural, and lymphatic tissues, the self-repair capacity of articular cartilage is limited once damaged [1,3,4]. This challenge is further exacerbated in hemophilic patients due to repeated intraarticular bleeding, deposits of hemosiderin, and a severe inflammatory microenvironment [6–9]. Unlike traumatic or degenerative cartilage defects, hemophilia patients commonly experience recurrent spontaneous intraarticular bleeding due to a lack of coagulation factor, resulting in the deposition of hemosiderin [10]. The deposition of hemosiderin can cause synovial hypertrophy and neovascularization, further increasing susceptibility to bleeding and mechanical injury [11]. Additionally, the deposition of hemosiderin can exacerbate the existing joint inflammatory response, increasing the expression of FGF23 and MMP-13 by releasing inflammatory factors, leading to the destruction of articular cartilage matrix and apoptosis of chondrocytes [10,12]. Furthermore, iron overload and lipid peroxidation caused by hemosiderin can directly trigger ferroptosis in chondrocytes [11–13]. While various approaches such as microfracture, autologous chondrocyte implantation, and arthroscopic debridement have been reported for cartilage defect repair, there is currently no integrated therapy specifically addressing early hemostasis, anti-inflammation, and long-acting chondrogenesis for hemophilic articular cartilage defects [3,7,14–17]. Given the unique challenges posed by repeated intraarticular bleeding, adverse inflammatory microenvironment, and poor cartilage regeneration ability in hemophilic patients, there is a need for innovative strategies to effectively promote cartilage regeneration and integration [6–9].

Hydrogel scaffold-based therapy has emerged as a promising strategy for cartilage repair due to their bionic microenvironments resembling the cartilage extracellular matrix (ECM) [1,15,18–21]. However, existing hydrogels lack consideration for the wet surface of intra-articular cartilage and often exhibit insufficient wet adhesion [1,14,18,20]. The past few years have witnessed a burgeoning interest in developing hydrogels with wet adhesion for *in situ* articular cartilage repair [1,20]. For instance, Zhang et al. reported an injectable exosomes-laden adhesive hydrogel with wet adhesion, exhibiting enhanced *in situ* cartilage regeneration [1]. Additionally, a multifunctional hydrogel demonstrated the ability to adhere to the wet cartilage surface, encapsulating exosomes and icariin to synergistically promote cartilage repair [20]. However, these studies primarily utilized normal rat models, and no hydrogel adhesive-based approach has hitherto been documented for repairing hemophilic articular cartilage defects, which presents additional challenges due to repeated intraarticular bleeding [1,6–9,20]. Ideally, to address this condition, hydrogel adhesives should exhibit properties such as injectability, quick *in situ* gelation to fill irregular cartilage defects, tight binding to wet tissue for local cavity hemostasis, and mechanical stability in the presence of repeated intra-articular bleeding [1,14,20,22]. An injectable self-healing natural biopolymer-based hydrogel adhesive, as reported by Zhou et al., may be a suitable candidate in this regard [23]. Composed of gelatin and chondroitin sulfate (CS), this biocompatible hydrogel adhesive has demonstrated strong tissue adhesion and excellent hemostatic abilities for rat livers, attributed to dynamic Schiff base bonds and hydrogen bonds [23]. Gelatin, a collagen hydrolysate, is widely used in biomedical fields due to its excellent biocompatibility, biodegradability, non-immunogenicity, and its ability to promote cell adhesion and

migration [24,25]. CS, as the main glycosaminoglycan (GAG) component of the cartilage ECM, has been reported to facilitate the production of cartilage matrix proteins and stimulate cartilage regeneration [1,18,26,27]. Furthermore, this hydrogel adhesive can be injected during minimally invasive surgery to target tissues, indicating its potential applicability during arthroscopy procedures [23]. Therefore, this injectable hydrogel adhesive may offer benefits for hemostasis and cartilage regeneration in hemophilic patients.

However, the effectiveness of ECM hydrogel adhesives for cartilage repair may be limited as they do not address the severe inflammatory microenvironment in hemophilic patients [6–9]. Bone marrow mesenchymal stem cells (BMSCs), known for their excellent chondrogenic and immunoregulatory properties, have been widely utilized to enhance cartilage regeneration and regulate inflammatory microenvironments [1,3,6,18,28]. Nonetheless, the *in vivo* implantation of BMSCs may potentially cause uncontrolled differentiation and stimulate chondrocyte hypertrophy and osteogenesis, thus unfavorable to cartilage repair [29–31]. There is an increasing consensus suggesting that the functional effects of BMSCs primarily occur through paracrine signaling, particularly via the secretion of exosomes [1,14,18,32,33]. These nanosized extracellular vesicles (30–200 nm) are rich in active molecules such as proteins, lipids, and miRNAs, inheriting the chondrogenic and anti-inflammatory properties of BMSCs, and engaging in intercellular communication with recipient cells [1,14,18,32–35]. Accordingly, BMSCs-derived exosomes have emerged as a promising cell-free therapeutic approach for hemophilic cartilage regeneration since they are safer and more effective than BMSCs [14,19,20,30]. In addition to BMSCs-derived exosomes, exosomes derived from normal chondrocytes have also been proven to promote the cartilage formation by increasing the ECM synthesis and regulating the chondrocytes proliferation and differentiation [29,36,37]. However, compared to BMSCs, it is difficult to obtain abundant normal chondrocytes, which may greatly restricts the clinical application of chondrocytes-derived exosomes [29,36,37]. Notably, exosomes secreted by degenerative chondrocytes could facilitate the apoptosis and inhibit the proliferation of chondrocytes [36,37]. Additionally, exosomes from chondrocytes experiencing aberrant biomechanical stimulation may cause abnormal calcification in cartilage tissue [38]. Besides, there is far less research on the mechanisms of chondrocytes-derived exosomes participating in the cartilage repair compared to BMSCs-derived exosomes [38]. Importantly, since it is critical to address severe inflammatory microenvironment in the repair process of hemophilic cartilage defect, exosomes from MSCs such as adipose MSC and BMSCs, may exert better anti-inflammatory effect than exosomes from other differentiated cells [18,39]. In line with this, an injectable adhesive hydrogel composed of gelatin and CS loaded with immunomodulatory and chondrogenic BMSCs-derived exosomes represents an appealing strategy to facilitate cartilage regeneration in individuals with hemophilia.

Building on these insights, we hypothesized that an injectable adhesive hydrogel laden with exosomes could synergistically promote effective cartilage repair by inducing early hemostasis, immunomodulation, and sustained chondrogenesis in hemophilic patients with cartilage damage. To validate this hypothesis, we developed a hydrogel adhesive loaded with BMSCs-derived exosomes, termed Hydrogel-Exos. This composite exhibited exceptional biocompatibility, biodegradability, swelling process, frictional coefficient, mechanical properties, wet tissue adhesiveness, hemostatic abilities, and prolonged exosome release, as illustrated in Fig. 1. The synthesis involved a straightforward combination of gelatin and aldehyde-functionalized chondroitin sulfate (oxidized CS, OCS) with the addition of borax. Exosomes were then

incorporated into the adhesive hydrogel network through noncovalent binding (hydrogen bonds), preserving their structure and bioactivity and ensuring a gradual and sustained delivery for cartilage repair. The adhesive hydrogel, endowed with dynamic Schiff base bonds and hydrogen bonds, demonstrated favorable injectability, self-healing capabilities, and tissue adhesion. This study comprehensively validated the micromorphological, mechanical, injectable, self-healing, swelling, frictional and adhesive properties, as well as the hemostatic behavior and exosome release of the Hydrogel-Exos composite. Additionally, a swine cartilage defect model was established to assess the injection feasibility, *in situ* gelling, and adhesiveness of the hydrogel adhesive under fluid-irrigated knee arthroscopy. Further investigations encompassed *in vitro* evaluations of biocompatibility, adhesion, migration, and activity of chondrocytes, as well as M1/M2 macrophage polarization on the Hydrogel-Exos. Moreover, *in vivo* assessments included the retention of exosomes, biocompatibility, and biodegradability of Hydrogel-Exos. Finally, we examined immunomodulation and cartilage regeneration *in vivo*, validating the therapeutic efficacy of Hydrogel-Exos in a full-thickness cartilage defect model in hemophilic rats.

## 2. Materials and methods

### 2.1. Preparation and culture of rats BMSCs, chondrocytes, and RAW264.7 cells

As previously described, BMSCs were extracted from 2-week-old rats' femurs and tibias by irrigating the marrow cavity under sterile conditions [18,32,33,40]. Primary BMSCs were cultured in Low glucose Dulbecco's modified Eagle medium (DMEM, Gibco, USA) supplemented with 10 % exosome-free fetal bovine serum (FBS, Gibco, USA) and  $1 \times$  penicillin-streptomycin and identified by Alizarin Red staining, Oil Red O staining, and Alcian Blue staining for osteogenic, adipogenic, and chondrogenic differentiation respectively). The second to the sixth generation of BMSCs was chosen for subsequent use.

Consistent with the prior studies, chondrocytes were obtained from 2-week-old rats' knee cartilage tissues [18,41]. The collected chondrocytes were cultured in high glucose DMEM with an addition of 10 % FBS (Gibco, USA) and  $1 \times$  penicillin-streptomycin at  $37^\circ\text{C}$  in 5 %  $\text{CO}_2$ . Similarly, the second to the sixth generation of chondrocytes was selected for subsequent utilization. RAW264.7 cells were acquired from the American Type Culture Collection (ATCC) cell bank and cultured under identical conditions to the chondrocytes.

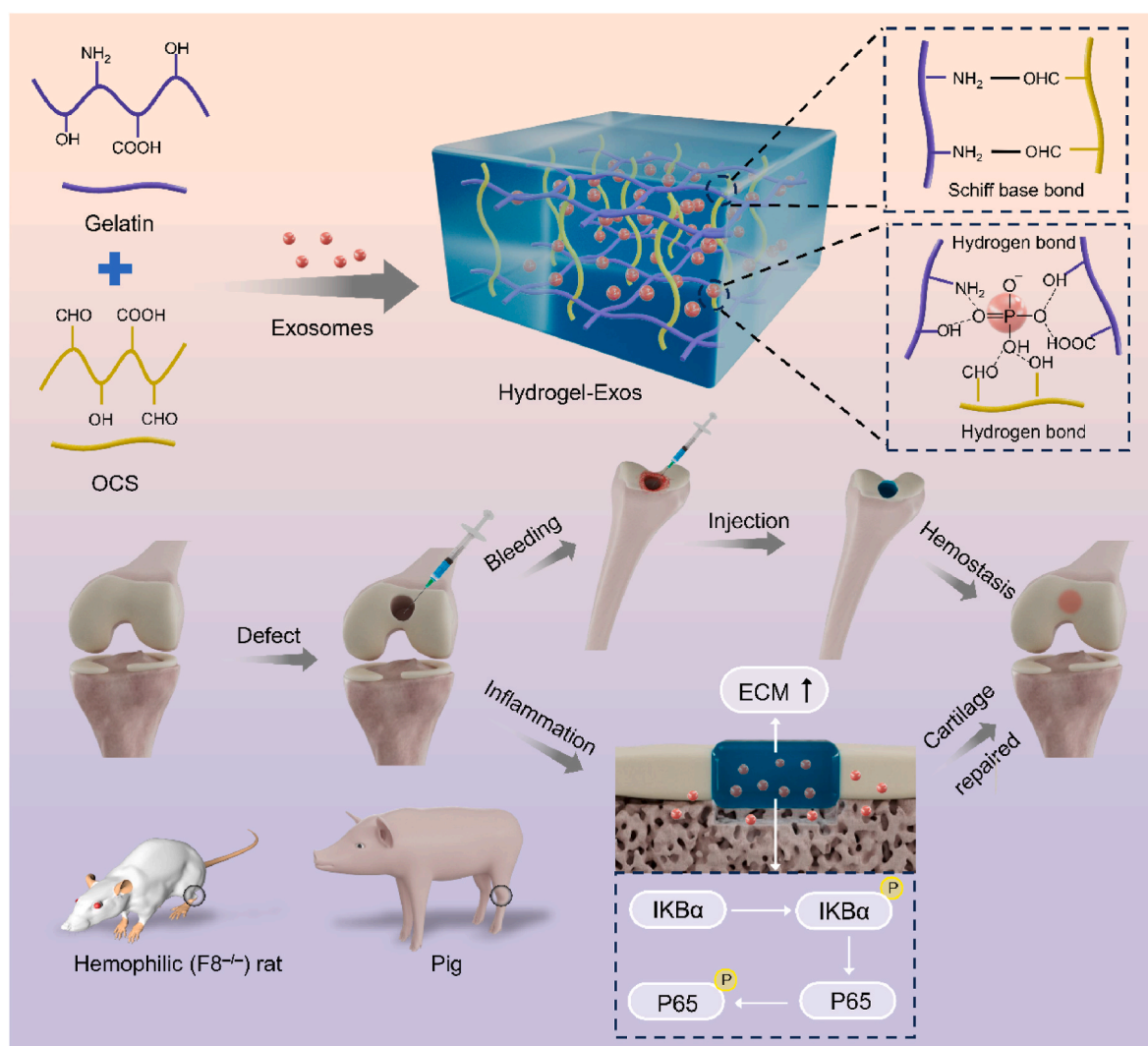


**Fig. 1.** The functional groups, chemical bonds, and fabrication of Hydrogel-Exos and its ability to achieve hemostasis, regulate inflammatory microenvironment, and promote cartilage regeneration after hemophilic articular cartilage defect.

## 2.2. Isolation and identification of exosomes derived from BMSCs

The cells' supernatant was collected for multistep ultracentrifugation after the BMSCs reached a confluence of 50–60 %, consistent with the literature [1,18,33]. In brief, the culture medium was centrifuged at 2000×g for 20 min and 10,000×g for 30 min at 4 °C to purify the supernatant. Next, the isolated exosomes were deposited in the bottom of the centrifuge tube after ultracentrifugation at 100,000×g for 90 min at 4 °C and were resuspended in 50 µL phosphate-buffered saline (PBS, Gibco, USA) for subsequent use. The morphological observation of exosomes was performed by transmission electron microscopy (TEM), while the particle size was determined by nanoparticle tracking analysis (NTA). Surface markers of exosomes, including TSG101 (ProteinTech, China), CD63 (Affinity, China), and Alix (ProteinTech, China) were detected by Western blot (WB) [33]. For the subsequent exosomes' endocytosis and spatial distribution assay, red fluorescent dye PKH26 (Sigma-Aldrich, USA) was used to stain exosomes according to prior protocols [32].

## 2.3. Establishment of Hydrogel-Exos system

### 2.3.1. Preparation of OCS

The preparation of OCS was based on our prior work [18,23]. Briefly, 5 g of CS (Aladdin, China) was completely dissolved in 80 mL of deionized (DI) water by stirring magnetically. Next, sodium periodate (Aladdin, China) solution was prepared by dissolving 1.93 g of crystalline powder in 20 mL of DI water and was added into the CS solution to react for 12 h with constant stirring at room temperature in the dark. Residual sodium periodate was neutralized by Ethylene glycol (98 %, Macklin, China) for 2 h. Then, the OCS solution was purified in DI water by a dialysis bag (3500 molecular weight cut-off) for 3 days. Finally, the dialysate was frozen at −80 °C for one day, followed by lyophilizing for one week to acquire the OCS powders. The degree of CS aldolization (oxidation CS) was evaluated through an iodometric titration.

### 2.3.2. Synthesis of gelatin-OCS adhesive hydrogel and Hydrogel-Exos composite

As described previously, the OCS solution (10 % w/v) was prepared by dissolving the OCS powders in borax (Aladdin, China) solution (0.05 M) [42]. Similarly, gelatin solution (30 % w/v) was obtained by dissolving gelatin (Aladdin, China) in borax solution at 65 °C. Then, an equal volume of OCS and gelatin solution were mixed at 37 °C to form gelatin-OCS adhesive hydrogels. According to prior works, 200 µg of BMSCs-derived exosomes were quickly dripped onto 100 µL of gelatin-OCS solution and stirred for 3 min to obtain the Hydrogel-Exos system [18]. The gelation time of the adhesive hydrogel with or without exosomes was assessed using a rotary rheometer (Physica MCR301, Anton Paar, Austria) by measuring the storage (elastic) modulus ( $G'$ ) and loss (viscous) modulus ( $G''$ ) and corresponding time once induced gelation through a time sweep pattern [23].

## 2.4. Characterization of Hydrogel-Exos composite

### 2.4.1. Scanning electron microscopy (SEM)

The samples' morphology detection was conducted by SEM (ZEISS Ultra 55, Germany) at 10,000 V acceleration voltage [18,32,42]. All samples were freeze-dried for 3 days and sputter-coated with platinum for 1 min before SEM observation.

### 2.4.2. Fourier transform infrared spectroscopy (FTIR)

A FTIR spectrometer (Nicolet IS10, Thermo Scientific, USA) was used to explore the functional groups and chemical structure of the samples [18,33,42]. The freeze-dried samples were pulverized and pressed into pieces before measurement via the specialized spectrum software.

### 2.4.3. Mechanical properties

The evaluation of the samples' rheological properties was performed utilizing a rotary rheometer (Physica MCR301, Anton Paar, Austria) with a dynamic oscillation frequency from 0.1 to 10 Hz and a constant strain of 1 % [18,23,42]. The storage (elastic) modulus ( $G'$ ) and loss (viscous) modulus ( $G''$ ) were determined based on the frequency-modulus curves. To examine the hydrogel's critical strain point, a strain (1–1000 %) amplitude sweep test was conducted. To assess the self-healing property of the adhesive hydrogel, an alternate strain sweep measurement was carried out at a constant frequency (1 Hz) at 37 °C. This step strain was altered from a smaller strain (5 %) to a larger strain (400 %) with a 200-s duration. A shear-thinning test in a frequency sweep mode was performed to evaluate the injectable property of the Hydrogel-Exos by determining the linear viscosity. A dynamic mechanical analyzer (DMA, Q800, TA Instruments, USA) was utilized to investigate the compressive strength of hydrogel samples from their strain-stress curve.

### 2.4.4. Injectability assessment

The pregel solution of Hydrogel-Exos labeled by Rhodamine was put in a syringe and injected into a culture dish and into an aqueous solution to assess its injectable properties [43,44]. In addition, a full-thickness porcine cartilage defect (7 mm in diameter and 2 mm in depth) model was established by a stainless-steel drill on a fresh femoral condyle to further observe the Hydrogel-Exos' injectability, *in situ* gel ability, and wet adhesiveness on cartilage tissue.

### 2.4.5. Self-healing property

To evaluate the self-healing properties of the Hydrogel-Exos hydrogel, two adhesive pieces with or without Rhodamine staining were cut into two parts, respectively. Next, one of the stained adhesive pieces was allowed to reconnect with another piece, which was not stained at 37 °C without any intervention.

### 2.4.6. Adhesiveness evaluation

To measure the adhesiveness of Hydrogel-Exos system, fresh porcine cartilage pieces (1 cm × 1 cm) were cut from femoral condyles purchased from a butcher. The porcine cartilage pieces were fixed on wooden blocks using Histoacryl cyanoacrylate adhesive (Golden Elephant 508, China) at room temperature for 30 min (Figs. S1A and B). After injection of 100 µL Hydrogel-Exos composite on a cartilage piece, the other cartilage piece was adhered for 20 min and formed a lap-shear or end-to-end manner [23,43,44]. A tensile mechanical test (Hengyi, HY-1080, Shanghai, China) was performed to measure the maximum adhesive strength when it breaks the lap-shear or end-to-end surface. Additionally, 500 g of weight was hung on the lap-shear specimen underwater to assess the wet adhesive strength. Besides, the end-to-end specimens were used to further investigate the adhesiveness and flexibility by separating and rotating them.

### 2.4.7. Knee arthroscopic operation *in vivo*

To further evaluate the injection feasibility, *in situ* gel formation, and adhesiveness of the adhesive hydrogel under fluid-irrigated knee arthroscopy, an arthroscopic procedure was conducted on a swine model using a basic arthroscopy setup (a Bebird video otoscope set, China) [22, 23]. A total of 6 four-month-old hybrid pigs (20–25 kg, 12 legs) were utilized in the present study. To reduce individual variability and the animal number, bilateral surgery was carried out [45]. Two small incisions (8 mm) were created on the lateral and medial side of the knee joint. A 30° arthroscope connected to a monitor was inserted into the joint cavity, and then continuous saline irrigation was introduced. After a 7 mm-diameter cartilage defect was created, the adhesive hydrogel was injected through a homemade hollow channel into the cartilage defect. Finally, the pigs were well-fed and allowed to move freely.

#### 2.4.8. In vitro exosome release profiles and encapsulation efficiency in Hydrogel-Exos

To explore the daily and cumulative release profiles of exosomes, a bicinchoninic acid (BCA) kit (Beyotime, China) was utilized as previously documented [18,33]. 100  $\mu$ L of Hydrogel-Exos, which contained 200  $\mu$ g of exosomes, was immersed in PBS solution at 37 °C and the supernatant was measured on 1, 3, 5, 7, 10, and 14 days to investigate the exosomes-releasing properties. The total amount of exosomes subtracted from the amount of released exosomes in the PBS was the amount of laden exosomes. The exosome encapsulation efficacy was calculated according to the following formulas [46] (1):

$$\text{Encapsulation efficacy (\%)} = \frac{\text{Amount of loaded exosomes}}{\text{Amount of total exosomes}} \times 100\% \quad (1)$$

#### 2.4.9. Endocytosis of exosomes

RAW264.7 cells and chondrocytes were respectively cultured on the Hydrogel-Exos for 24 h to explore the cell endocytosis of exosomes after staining by PKH26 [1,18,33]. Next, cells underwent fixing, membrane-breaking, blocking, and staining by Actin Tracker Green (Beyotime, China) and Hoechst 33342 (Sigma, USA) for final observation under a laser confocal microscope (ZEISS LSM 980, Germany).

#### 2.4.10. Friction test for the Hydrogel-Exos

To simulate the friction property of Hydrogel-Exos on the articular cartilage surface, a reciprocating sliding tribological measurement was conducted on a high-frequency reciprocating friction and wear tester (MGW-001, Jinan Yihua Tribology Testing Technology Co. LTD, China). This tester was mainly composed of a bottom surface (stainless-steel disk) and a top surface (polyethylene sphere). The oscillation amplitude, reciprocating frequency, loading force, and duration time were set as 4 mm, 1 Hz, 1 N, and 600 s, respectively [47–50].

#### 2.4.11. Swelling behavior of the Hydrogel-Exos

The Hydrogel-Exos was immersed in PBS at 37 °C for 4 days to assess its swelling process. To determine the swelling ratio, the dried weight ( $W_0$ ) of samples was first recorded, followed by measuring the weight change of the hydrogels twice a day [44]. The swelling ratio was calculated based on the subsequent equation (2):

$$\text{Swelling ratio (\%)} = \frac{W_t - W_0}{W_0} \times 100\% \quad (2)$$

where  $W_t$  and  $W_0$  represents the wet weight at predefined time and initial dried weight, respectively.

### 2.5. In vitro experiments

#### 2.5.1. Cell biocompatibility evaluation

To assess the cell biocompatibility of Hydrogel-Exos, we performed live/dead staining, cell counting kit-8 (CCK-8, Beyotime, China), and cytoskeletal staining tests [18,33,51]. Briefly, cell viability was measured by a live/dead staining test after the seeding of  $5 \times 10^5$  chondrocytes and RAW264.7 cells on each sample for 1 d, respectively. Subsequently, PBS, calcein-AM (Invitrogen, USA), and propidium iodide (PI, Invitrogen, USA) were used to prepare the live/dead solution, which was co-incubated with each sample for 30 min. The viability results were observed under a laser confocal microscope (ZEISS LSM 980, Germany). For the assessment of cell proliferation,  $5 \times 10^5$  chondrocytes and RAW264.7 cells were separately seeded on each sample for 1, 3, and 7 days and incubated with CCK-8 solution (100  $\mu$ L/mL) for 2 h. Subsequently, the optical density (OD) value was measured by an enzyme labeling instrument (BioTech, Germany) at 450 nm wavelength after 100  $\mu$ L supernatant was transferred into a 96-well plate. The chondrocyte adhesion was examined via a cytoskeletal staining test after labeling with Actin Tracker Green (Beyotime, China) and Hoechst 33342 (Beyotime, China). Glass bottom cell culture dishes used in this study

were purchased from NEST Biotechnology Co. Ltd. (Wuxi, China).

#### 2.5.2. Cell migration test

It has been widely acknowledged that chondrocyte migration is crucial for the repair of cartilage defects [40,52]. Consequently, to evaluate chondrocyte migration ability on Hydrogel-Exos, a longitudinal scratch was created on chondrocytes' surface after their confluence reached about 90 % and cultured for 12 h and 24 h. Next, PBS was used to wash the detached cells. Finally, Calcein AM (Invitrogen, USA) staining was conducted before visualization under a laser confocal microscope (ZEISS LSM 980, Germany).

#### 2.5.3. Construction of Hydrogel-Exos/RAW264.7 cells/chondrocytes integrated culture system

To explore whether the immune microenvironment regulates the fate of chondrocytes, an Hydrogel-Exos/RAW264.7 cells/chondrocytes integrated culture system was constructed in a Transwell chamber (ThermoFisher Scientific, USA) [1,18,40]. The chondrocytes were pre-treated with IL-1 $\beta$  (10 ng/mL) 1 d before the assay. As exhibited in Figs. 6A and 1  $\times 10^5$  RAW264.7 cells was seeded on Hydrogel-Exos in the lower chamber, and  $1 \times 10^4$  chondrocytes were cultured in the upper chamber. In order to allow the free exchange of cytokines, a 3.0  $\mu$ m pore size polycarbonate membrane was selected to separate the two compartments.

#### 2.5.4. Gene expression

The total cellular RNA was acquired with a Simply P Total RNA Extraction Kit (BioFlux, China), followed by reverse transcription into cDNA using an all-in-one reverse transcription kit (TOLOBIO, China) for final real-time qPCR (RT-qPCR) on the QuantStudio 5 (Thermo Fisher, USA) [51]. This experiment was performed thrice before statistical analysis using the  $2^{-\Delta\Delta C_t}$  method. The primers of each gene are displayed in Table 1.

#### 2.5.5. Immunofluorescence (IF)

For this assay, cells were fixed in 4 % paraformaldehyde for 30 min, permeabilized in 0.5 % Triton X-100 (Biofroxx, Germany) for 30 min, and blocked in 3 % bovine serum albumin (BSA, Biofroxx, Germany) for 1 h at room temperature. Subsequently, they were reacted in specific primary antibodies overnight at 4 °C (Table 2), in secondary antibodies for 1 h at normal temperature, and then in Hoechst 33342 (Beyotime, China) for 5 min. The samples were washed with PBS thrice between each step. Finally, the fluorescence images were captured utilizing a laser confocal microscope (ZEISS LSM 980, Germany).

#### 2.5.6. WB experiment

Proteins were extracted by dissolving cells in a lysis solution containing radio-immunoprecipitation assay (RIPA, CWBIO, China) buffer added with phosphatase and protease inhibitors (KeyGEN, China) on ice for 30 min [18,33,40,51]. After the determination of total protein concentration using a BCA kit (Beyotime, China), it was denatured by loading buffer (Beyotime, China) at 100 °C for 10 min. After that, equal amounts (20  $\mu$ g) of protein were separated by sodium dodecyl sulfate-polyacrylamide gel electrophoresis (SDS-PAGE, Beyotime,

**Table 1**  
Primer sequences of each gene.

Target	Forward	Reverse
GAPDH	AGACAGCCGCATCTTCTTGT	CTTCCGTGGGTAGAGTCAT
COL-2	AACCCAAAGGACCCAAATAC	CCGACTGTGAGGTTAGGAT
SOX-9	CGTGGTGACAAGGGTGAGAC	TAGGTGATGTTCTGGGAGGC
MMP-13	AGGCCTTCAGAAAAGCCTTC	GAGCTGCTTGCCAGGTTTC
Arg-1	CTCCAAGCCAAAGTCTTAGAG	GGAGCTGTATTAGGGACATCA
IL-10	CTTACTGACTGGCATGAGGATCA	GCAGCTTAGGAGCATGTGG
iNOS	GTTCTCAGCCCAACAATACAAGA	GTGGACGGGTGATGTGAC
TNF- $\alpha$	CGAGTGACAAGCCTGTAGCC	ACAAGGTACAACCCATCGGC

**Table 2**  
Information on primary antibodies used.

Antibodies	Species	Type	Dilution (IF/IHC, WB)	Source
Anti-GAPDH	Rabbit	Polyclonal IgG	1:8000	ProteinTech, China
Anti-COL-2	Rabbit	Polyclonal IgG	1:200/1:200, 1:1000	Affinity, China
Anti-SOX-9	Rabbit	Polyclonal IgG	1:1000	Affinity, China
Anti-MMP-13	Rabbit	Polyclonal IgG	1:200/1:200, 1:2000	ProteinTech, China
Anti-Arg-1	Rabbit	Polyclonal IgG	1:200, 1:5000	ProteinTech, China
Anti-iNOS	Rabbit	Polyclonal IgG	1:200/1:200, 1:1000	GeneTex, America
Anti-IKB $\alpha$	Mouse	Monoclonal IgG	1:1000	CST, America
Anti-p-IKB $\alpha$	Rabbit	Monoclonal IgG	1:1000	CST, America
Anti-P65	Rabbit	Monoclonal IgG	1:1000	CST, America
Anti-p-P65	Rabbit	Monoclonal IgG	1:1000	CST, America
Anti-Alix	Rabbit	Polyclonal IgG	1:2000	ProteinTech, China
Anti-CD63	Rabbit	Polyclonal IgG	1:1000	Affinity, China
Anti-TSG101	Mouse	Monoclonal IgG	1:5000	ProteinTech, China
Anti-Calnexin	Rabbit	Polyclonal IgG	1:2000	ProteinTech, China

China), transferred onto the polyvinylidene difluoride (PVDF, Thermo Fisher, USA) membranes, and blocked in high-efficiency blocking buffer (Genefist, China) for 15 min. Next, primary antibodies (Table 2) and secondary antibodies were successively applied to incubate with the PVDF membranes. After being immersed in an enhanced chemiluminescence (ECL, Thermo Fisher, USA) solution, the protein bands were observed under the GelView 6000 Pro (BLT, China). Ultimately, protein band density was quantified by ImageJ software.

## 2.6. *In vivo* experiments

### Ethical statement

All animal studies were conducted in strict accordance with the guidelines outlined in the National Institutes of Health Guide for the Care and Use of Laboratory Animals. The research protocols were comprehensively reviewed and approved by the Animal Experimental Ethics Committee of Southern Medical University Nanfang Hospital.

### 2.6.1. Establishment of hemophilic rat cartilage defect model

Adult female F8<sup>-/-</sup> rats (250–300 g) were obtained from the Shanghai Model Organisms Center, Inc. and randomly assigned into four groups, including untreated control group (defects without treatment, n = 10), pure adhesive hydrogel group (Hydrogel, n = 10), pure exosomes group (Exos, n = 10), and exosomes-loaded adhesive hydrogel group (Hydrogel-Exos, n = 10). The genotypes of the rat were determined by qPCR analyses of genomic DNA extracted from rat-tail snips using the following primers: forward, 5'-TCA CCC GTG CAT AAC AGG ACA GAC-3' and reverse, 5'-CCG GGG GCA TGC GAT TTT TC-3' [53,54]. The hemophilic cartilage defect model was constructed according to prior descriptions of normal rats [1,2,4,45,55]. After anesthesia via intraperitoneal injection of pentobarbital (40 mg/kg), a middle incision was created on the left knee joint. Subsequently, a full-thickness cartilage defect of 2 mm in diameter and 1 mm in depth was made at the middle of the femoral trochlear. In the Hydrogel group and Hydrogel-Exos group, samples were separately injected into the defect. The defect area in the exosomes group was administrated with 200  $\mu$ g exosomes in PBS. The joint capsule, muscle, and skin were closed sequentially. After the operation, the rats were allowed to move freely

and well-fed in a warm environment.

### 2.6.2. Pain measurements

Pain measurements, which included mechanical allodynia and thermal hyperalgesia assay, were conducted to evaluate joint function restoration before (12 h) and after surgery (1, 2, 3, 4, 5 and 6 weeks) [56–58]. Animals were acclimated to the equipment and surroundings for 20 min before testing.

Mechanical allodynia was determined by placing animals on a metal mesh in a cubicle and recording the paw withdrawal threshold (PWT) with incremental forces elicited by von-Frey filaments (4, 6, 8, 10, 15, 26, 60, 100 and 180 g). The force needed to induce the lifting, biting or licking of the posterior paw was recognized as a threshold for positive response. Each rat was repeatedly stimulated five times at a 2-min interval. A decrease of PWT indicated an increase in mechanical allodynia or pain aggravation. Fig. 11A is a schematic illustration depicting the von-Frey testing.

Thermal sensitivity measurement could be conducted by placing rats on a heat conduction plate in a cubicle and allowing their hind paws to touch a hot plate (56 °C). The time required to elicit the licking or raising of the posterior paw was recorded as thermal withdrawal latency (TWL). Similarly, each animal was repeatedly exposed five times at a 2-min interval to avoid scalding tissues. Consistently, a decrease of TWL represented an increase in thermal sensitivity or pain aggravation. Fig. 11D is a schematic illustration depicting the hot plate testing.

### 2.6.3. Gait analysis

The gait analysis was also carried out to assess the joint function recovery 2, 4, and 6 weeks after the surgery [51,59,60]. The rats were allowed to walk on papers after coating their hind limbs in blue ink. As depicted in Fig. 11G, the sciatic function index (SFI) was calculated based on the following formula by measuring three footprint parameters, which included print length (PL), toe spread (TS), and intermediate toe spread (ITS) (3):

$$\text{SFI} = -38.3 \times \frac{(\text{PL}_{\text{Exp}} - \text{PL}_{\text{Ctrl}})}{\text{PL}_{\text{Ctrl}}} + 109.5 \times \frac{(\text{TS}_{\text{Exp}} - \text{TS}_{\text{Ctrl}})}{\text{TS}_{\text{Ctrl}}} + 13.3 \times \frac{(\text{ITS}_{\text{Exp}} - \text{ITS}_{\text{Ctrl}})}{\text{ITS}_{\text{Ctrl}}} - 8.8 \quad (3)$$

where Exp and Ctrl indicate the experimental and control limbs, respectively.

### 2.6.4. Hemolysis test and *in vivo* biocompatibility

The hemocompatibility of Hydrogel-Exos was assessed through a hemolysis test. During this procedure, each sample was incubated with whole rat blood at 37 °C for 4 h. Triton-100X and PBS were included as positive and negative control groups, respectively. Subsequently, the centrifuge tubes were spun at 10,000 g for 5 min at 4 °C. Following the determination of supernatant absorbance at 540 nm using an enzyme-labeling instrument (BioTech, Germany), the hemolysis percentage was calculated using the following equation (4):

$$\text{Hemolysis (\%)} = \frac{\text{OD}_{\text{Sample}} - \text{OD}_{\text{PBS}}}{\text{OD}_{\text{Triton}} - \text{OD}_{\text{PBS}}} \times 100\% \quad (4)$$

where OD represents the optical density.

Besides, the levels of alanine aminotransferase (ALT), aspartate aminotransferase (AST) and total protein (TP) were determined to examine the *in vivo* biocompatibility of samples after obtaining the whole rats blood at the end of 6 weeks treatment. Five major organs, including the heart, lung, kidney, liver and spleen, were harvested and stained with hematoxylin-eosin (H&E) for pathological examination [33,51].

### 2.6.5. *In vivo* evaluation of exosome retention

To further investigate the *in vivo* exosome retention,

bioluminescence imaging was applied [32]. Briefly, exosomes labeled with PKH26 fluorescence dye were incorporated into Hydrogel-Exos and subsequently implanted into the cartilage defect on the left knee. Subsequently, rats were subjected to noninvasive imaging using the Spectral Instruments Imaging system (Ami, HTX, USA) on days 0, 3, 7, 14, and 21.

#### 2.6.6. *In vivo* degradation of the Hydrogel-Exos

To explore the *in vivo* degradation behavior of Hydrogel-Exos, 1 mL of Cy7-labeled sample was subcutaneously injected into the back of rats [32,43,44]. Similarly, the fluorescence intensity was visualized and recorded using the Spectral Instruments Imaging system (Ami, HTX, USA) on days 0, 3, 7, 14, and 21. Furthermore, rats were euthanized on days 0, 3, 7, 14, and 21, respectively, and the surrounding tissues of the samples were dissected for subsequent macroscopic observation and histological analysis using H&E staining. The degradation profile was quantified by relative volume and mass change and calculated based on the following equation, (5) and (6) respectively [22]:

$$\text{Relative volume (\%)} = \frac{V_t}{V_0} \times 100\% \quad (5)$$

where  $V_t$  and  $V_0$  represents the volume obtained in predefined day and day 0, respectively.

$$\text{Relative mass (\%)} = \frac{W_t}{W_0} \times 100\% \quad (6)$$

where  $W_t$  and  $W_0$  represents the weight obtained in predefined day and day 0, respectively.

#### 2.6.7. Assessment of *in vivo* hemostatic capacity

It is well-established that repeated intraarticular bleeding has detrimental effects on cartilage defect repair in hemophilic patients [6–9]. Therefore, alongside the assessment of wet adhesiveness, the hemostatic ability of Hydrogel-Exos was evaluated *in vivo*. Adult female F8<sup>-/-</sup> rats (250–300 g) were employed to establish models involving liver hemorrhage, rat-tail amputation, and femoral condyle drilling [23, 44,61,62]. In the liver hemorrhage model, the liver was exposed after anesthesia through intraperitoneal administration of pentobarbital (40 mg/kg). Given that the leaked blood may be encapsulated in the adhesive hydrogels, leading to an incorrect calculation of blood loss, commercial gauzes and adhesive hydrogels were weighed before the liver hemorrhage and rat-tail amputation experiments for the precise calculation of blood loss. Gauzes were positioned under the liver for blood collection before inducing liver hemorrhage. A 0.5 cm V-shaped incision was made on the liver with a scalpel, and Hydrogel-Exos were applied at the bleeding site. Untreated and fibrin glue-treated groups served as controls, and the total blood loss was calculated based on the weight increase of the gauzes and adhesive hydrogels within 3 min. In the tail amputation model, rat tails were amputated within 1 cm of the tip using surgical scissors, and the subsequent procedure was consistent with the liver hemorrhage model. In the femoral condyle drill model, after exposing the left knee joint, a full-thickness cartilage defect (2 mm in diameter and 1 mm in depth) was created, and Hydrogel-Exos were utilized to attach and fill the bleeding defect.

#### 2.6.8. Gross observation, micro-CT examination, histological evaluation and immunohistochemistry

After a 6-week treatment period, the animals were euthanized, and their femurs were harvested. Initially, the gross appearance of the cartilage defect was documented using a magnified photography system. Subsequently, the femurs were fixed in 4 % paraformaldehyde for 24 h, and scanned by the micro-CT (Scanco mCT50, Switzerland) to assess the subchondral bone formation. The center of the defect area was defined as the region of interest (ROI) for quantification of osteogenesis parameters, including bone volume/tissue volume (BV/TV), trabecular

number (Tb.N), trabecular thickness (Tb.Th) and trabecular separation (Tb.Sp). Then, the samples were decalcified in a decalcifying solution for one month, embedded in paraffin, and sectioned at a thickness of 5  $\mu$ m in the sagittal direction. Various staining techniques were employed for histological analysis: H&E staining assessed morphology, safranin-O/fast green (Saf-O) staining evaluated glycosaminoglycan (GAG) deposition, Masson trichrome staining (MTS) detected collagenous fibers and immunohistochemical staining was employed to examine the expression of collagen type II (COL-2), matrix metalloproteinase-13 (MMP-13), and inducible nitric oxide synthase (iNOS) [18,45]. The primary antibodies used are listed in Table 2. Additionally, Perls' Prussian Blue staining was utilized to detect the deposition of hemosiderin in articular cartilage defect lesions from normal and hemophilic rats.

#### 2.7. Statistical analysis

Statistical analyses were performed using SPSS Statistics 23.0 (IBM, USA) and GraphPad Prism 8.0 (GraphPad Software, USA). Unpaired t-tests were employed for two-group comparisons, while one-way analysis of variance (ANOVA) with Bonferroni's test was utilized for three or more groups. All experimental results were presented as mean  $\pm$  standard deviation (Mean  $\pm$  SD). A P-value <0.05 was statistically significant.

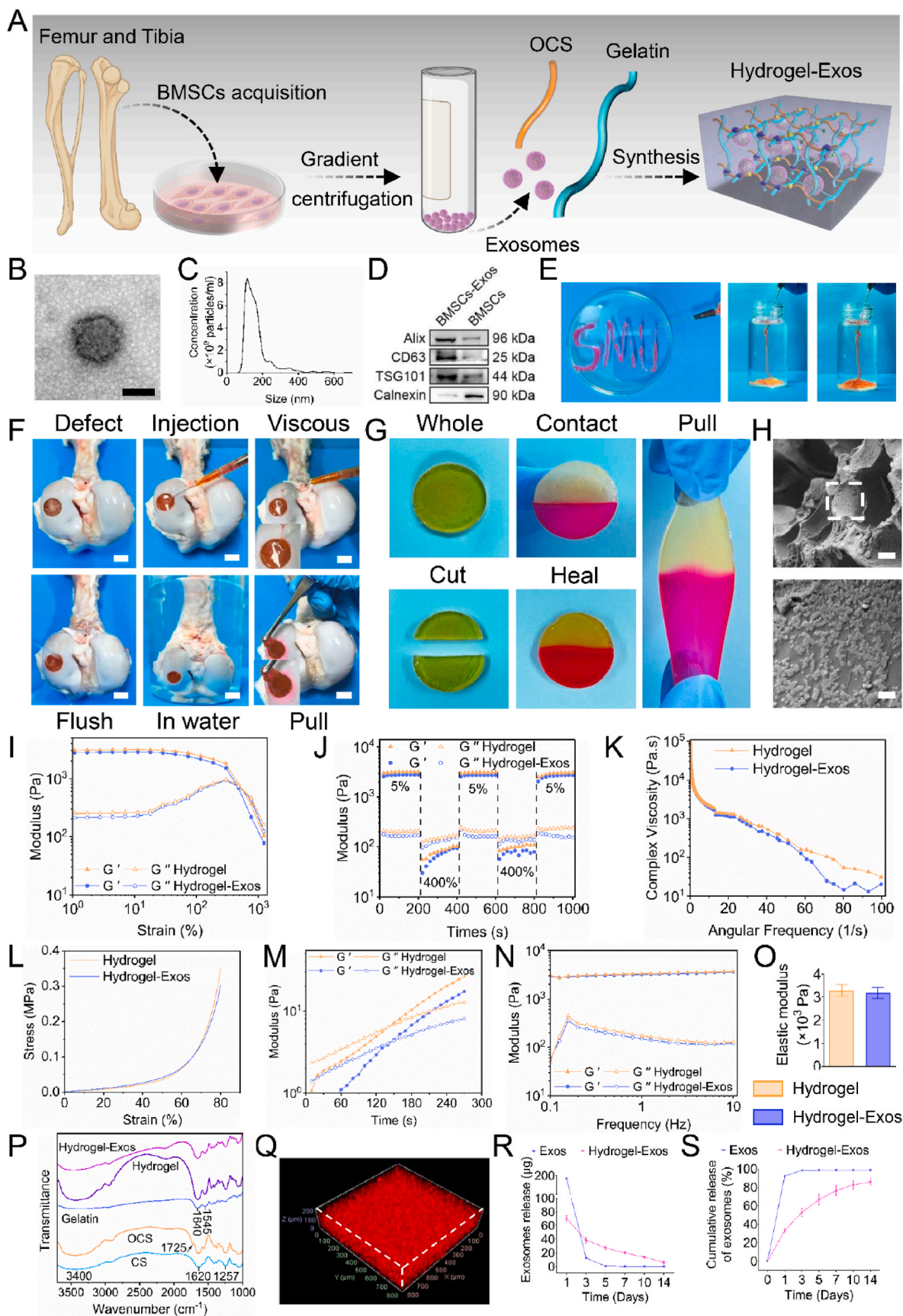
### 3. Results and discussion

#### 3.1. Characterization of BMSCs-derived exosomes

The isolation process of BMSCs-derived exosomes is briefly illustrated in Fig. 2A. To confirm the successful isolation of exosomes from BMSCs, various techniques, including TEM, NTA, and WB for specific surface markers, were employed. As depicted in Fig. 2B, TEM image revealed a spherical vesicle with a teacup-like shape, characteristic of exosomes. Consistent with TEM results, NTA technology determined the average particle size of vesicles to be approximately  $165.4 \pm 79.7$  nm (Fig. 2C). Moreover, WB results demonstrated a significant increase in the expression of specific surface markers, including TSG101, CD63, and Alix proteins, on the acquired vesicles, compared to BMSCs. However, these vesicles lacked Calnexin (Fig. 2D) [63–65]. These findings collectively confirmed the successful isolation of exosomes from BMSCs.

#### 3.2. Fabrication and characterization of Hydrogel-Exos

The material preparation process and simple chemical component of the Hydrogel-Exos are illustrated in Fig. 2A. The adhesive hydrogel is fabricated via self-crosslinking of gelatin and periodate oxidized CS after the addition of borax based on our previous studies [23,42]. CS, being water-soluble, typically requires blending with other biopolymers like collagen and chitosan for chemical crosslinking to create stable hydrogels [42]. The degree of CS aldolization (oxidation CS) is about 90 %, as determined by an iodometric titration of the periodate in the reaction system (Table S1). Moreover, the rapid degradation of gelatin at 37 °C (physiological temperature) limits its widespread *in vivo* application for long-term repair [42]. Gelatin has been reported to interact with OCS, forming an adhesive hydrogel through the Schiff base reaction between the amino groups of gelatin and the aldehyde groups in OCS in the presence of borax [23,42]. Borax plays a crucial role in this Schiff base reaction by interacting with OCS through the borate-diol complexation [23,42]. This interaction allows gelatin to crosslink with OCS, leading to the formation of an adhesive hydrogel without the need for additional toxic crosslinking agents [23,42]. Subsequently, BMSCs-derived exosomes were encapsulated into the adhesive hydrogel network, establishing the Hydrogel-Exos system through the formation of hydrogen bonds between the phosphate groups on the exosomes' phospholipid surface and the numerous hydroxyl, aldehyde, carboxyl, and amine groups provided by OCS and gelatin (Fig. S2) [23,42].



(caption on next page)

**Fig. 2.** Characterization of the Hydrogel-Exos composite. (A) Illustration of the fabrication and structure of the Hydrogel-Exos system. (B) Morphology of acquired nanoparticles (exosomes) determined by transmission electron microscopy (TEM). Scale bar represents 100 nm. (C) Nanoparticle tracking analysis (NTA) characterized the size range of nanoparticle (exosomes). (D) BMSCs-Exos surface-specific makers, including TSG101, CD63, and Alix proteins, and a negative control (Calnexin) were assessed by Western blot (WB). (E) Photographs showing the rhodamine-dyed Hydrogel-Exos could be injected into a culture dish and into the water using a syringe. (F) Rhodamine-dyed Hydrogel-Exos hydrogel precursor could also be smoothly injected into the porcine cartilage defect site, gelled *in situ*, and adhered with surrounding tissues with or without a water environment. Scale bar: 5 mm. (G) Images exhibiting the macroscopic self-healing property of Hydrogel-Exos. (H) The microstructure of the Hydrogel-Exos system was detected by scanning electron microscopy (SEM). Scale bar: 10  $\mu\text{m}$  (at low magnification), and 1  $\mu\text{m}$  (at high magnification). (I) The strain amplitude sweep test (1–1000 %) at a constant frequency (1 Hz) at 37 °C. (J) Demonstration of rapid self-healing behavior of Hydrogel-Exos via continuous step strain (5 % strain to 400 % strain to 5 % strain) measurements. (K) Shear-thinning measurement of Hydrogel-Exos. (L) Cyclic compression curves of Hydrogel-Exos. (M) Dynamic time sweep rheological detection to assess gelation kinetics of Hydrogel-Exos. (N) Rheological properties of adhesive with or without exosomes. (O) Graph of the quantitative analysis of mechanical properties of adhesive and Hydrogel-Exos ( $n = 3$ ). (P) FTIR spectra of chondroitin sulfate (CS, bluish), OCS (oxidized chondroitin sulfate, orange), gelatin (light purple), adhesive hydrogel (deep purple) and Hydrogel-Exos (red). (Q) 3D immunofluorescence image exhibited that exosomes labeled by PKH26 were evenly distributed in the adhesive hydrogel, and the penetration depth of the exosomes was about 200  $\mu\text{m}$ . (R) The daily release profile of exosomes with or without adhesive hydrogel for 14 days ( $n = 3$ ). (S) The cumulative release curve of exosomes with or without adhesive hydrogel for 14 days ( $n = 3$ ). Statistical differences were determined by utilizing One-way ANOVA with Bonferroni's multiple comparison tests when comparing three or more groups. When comparing two groups, the unpaired *t*-test was utilized. (\* $P < 0.05$ , \*\* $P < 0.01$ , and \*\*\* $P < 0.001$ ).

Injectability is crucial for the application of adhesive hydrogel during minimally invasive procedures, including arthroscopy [23]. As observed in Fig. 2E, the rhodamine-dyed Hydrogel-Exos hydrogel precursor could be continuously injected into a culture dish and into a bottle filled with water using a syringe, maintaining a stable gel state without dissolution. Additionally, this Hydrogel-Exos hydrogel precursor could be smoothly injected into the porcine cartilage defect site, demonstrating desirable *in situ* gelling, molding, well-fitting, integrating, and wet adhesiveness properties after being flushed by water or immersed in water (Fig. 2F). It is well-established that adhesive hydrogels commonly face external mechanical force after transplantation at the defect site, which may accelerate their degradation, limit their lifespan, and alter their properties [23,43]. Accordingly, the self-healing properties of the Hydrogel-Exos composite were evaluated. As depicted in Fig. 2G, the full moon-shaped adhesive hydrogel was first cut into two semilunar-shaped pieces, with one of them dyed red. These two pieces were then brought into contact at 37 °C for 20 min, successfully merging and healing. Importantly, the healed adhesive hydrogel could withstand external force and maintain integrity. SEM imagings exhibited a porous hydrogel structure with abundant exosomes embedment (Fig. 2H). Additionally, a strain amplitude sweep experiment on the hydrogel with or without exosomes revealed that the storage modulus ( $G'$ ) and loss modulus ( $G''$ ) of the samples slightly changed when the strain reached up to 100 %, indicating the samples' ability to maintain significant elastic deformations (Fig. 2I). However, with increasing strain, the values of  $G'$  and  $G''$  significantly declined and became equal at around 400 % strain, indicating that both the hydrogels could transition into a sol state when the external force exceeded the critical strain. Subsequently, continuous cyclic strain measurement demonstrated the recoverability of the Hydrogel-Exos and pure adhesive hydrogel (strain from 5 % to 400 % and back to 5 %) at a constant frequency of 1 Hz. As shown in Fig. 2J, the hydrogels transformed into a sol state ( $G' < G''$ ) at a critical strain of 400 %, returning to a gel state again once the strain reverted to 5 % ( $G' > G''$ ). These results suggest that the Hydrogel-Exos and pure adhesive hydrogel possess quick and significant self-healing properties due to the presence of dynamic covalent Schiff-base bonds and reversible hydrogen bonding [23]. In recent years, injectable hydrogels with self-healing and *in situ* crosslinking properties have gained great attention in cartilage tissue engineering [66]. Compared with traditional crosslinked hydrogel, self-healing hydrogel can extend its lifetime and provide adaptability to alterations in the structural network for cell proliferation and gel degradation [66,67]. Moreover, given that the articular cartilage defect commonly occurs in areas with frequent movements and experiences excessive local stress, self-healing ability can efficiently recover the structural integrity of hydrogels and dissipate energy around weight-bearing regions, thereby prolonging the duration of hydrogels and making them suitable for articular injection [20,66–70]. In addition, the viscosity test result revealed that the increment of shear rate reduced the viscosity (Fig. 2K),

likely due to the shear behavior breaking the dynamic hydrogel network that contributes to the injectability and self-healing of the hydrogels [23]. Moreover, the cyclic compression measurement finding demonstrated that the compressive modulus of the Hydrogel-Exos was approximately 0.3 MPa when the strain reached 80 % (Fig. 2L), within the range of compressive modulus of native human articular cartilage (0.24–1 MPa) [71–74]. It is well-established that the gelation time of the adhesive hydrogels is crucial for *in vivo* application. The results of time sweep rheological tests showed that the gelation times of the adhesive hydrogel with or without exosomes were approximately 150 s, indicating that the adhesive hydrogel has a relatively rapid gelation time, which is consistent with prior reports and not influenced by the embedding of exosomes (Fig. 2M) [23,42]. The Schiff base reaction between the amino groups of gelatin and the aldehyde groups in OCS and their internal hydrogen bonds can account for the quick gelation of this adhesive hydrogel [23,42].

It is widely acknowledged that the mechanical characteristics of the extracellular matrix can significantly impact cell differentiation and fate [33,51]. Therefore, the mechanical properties of the adhesive hydrogel, with or without exosomes, were investigated through frequency sweep tests. Over a frequency range of 0.1–10 Hz, the elastic modulus (storage modulus  $G'$ ) of both adhesive hydrogels exceeded the viscous modulus (loss modulus  $G''$ ) (Fig. 2N), indicating their stability and viscoelastic nature. Additionally, the average  $G'$  of Hydrogel-Exos (3177.86  $\pm$  230.65 Pa) was comparable to pure adhesive hydrogel (3292.38  $\pm$  258.37 Pa) (Fig. 2O), suggesting that the encapsulation of exosomes had minimal impact on the mechanical properties of the adhesive. These results cooperate with the cyclic compression measurement, providing appropriate mechanical support for articular cartilage regeneration [67]. FTIR analysis was employed to characterize the functional groups in gelatin and OCS (Fig. 2P). The typical peaks of gelatin at 1640  $\text{cm}^{-1}$  and 1545  $\text{cm}^{-1}$  corresponded to C=O stretching (amide I) and N–H bending (amide II), respectively [42,75,76]. The characteristic peaks in the CS spectrum at 3400, 1620, and 1257  $\text{cm}^{-1}$  were attributed to the –OH of carbohydrate, –COOH, and S=O stretching, respectively [77,78]. After oxidation with sodium periodate, the –OH on the CS was partially transformed to –COH, confirmed by FTIR analysis with a new peak observed at 1725  $\text{cm}^{-1}$  in the OCS spectrum compared to CS (Fig. 2P) [18]. The adhesive hydrogel spectrum displayed typical peaks of the primary bonds and groups, indicating the successful fabrication of the adhesive hydrogel based on gelatin and OCS. Furthermore, after the formation of Schiff base bond, the characteristic peak of OCS at 1725  $\text{cm}^{-1}$  disappeared, and a peak at 1590–1690  $\text{cm}^{-1}$  of imine bond (–C=N) was observed. Similarly, a wider and stronger peak at 1590–1690  $\text{cm}^{-1}$  (–C=N) was present in the adhesive hydrogel spectrum compared to the gelatin due to the numerous Schiff base cross-linking (Fig. 2P) [79–81]. The absorption peak at 3200–3500  $\text{cm}^{-1}$  in the Hydrogel-Exos spectrum was slightly shifted compared to the pure hydrogel, indicating the hydrogen bond formation between exosomes

and hydrogel (Fig. 2P) [79–81]. To explore the 3D distribution of exosomes in the adhesive hydrogel, PKH26-labeled exosomes loaded onto the hydrogel were visualized under confocal reflection microscopy. The 3D immunofluorescence results demonstrated the homogeneous distribution of exosomes in the adhesive hydrogel, confirming the successful encapsulation of BMSCs-derived exosomes (Fig. 2Q). The encapsulation efficiency of exosome in Hydrogel-Exos was  $85.8 \pm 3.9\%$ . Finally, *in vitro* exosome release from Hydrogel-Exos was investigated over 2 weeks. As shown in Fig. 2R and S, more than 80 % of the exosomes were cumulatively released from Hydrogel-Exos over 14 days, enabling the exosomes to exert their immunomodulatory and repair effects during articular cartilage injury. The sustained-release properties of Hydrogel-Exos can be attributed to the formation of reversible non-covalent binding (hydrogen bonds) between exosomes and the adhesive hydrogel [23,33,42].

It has been well-established that the articular cartilage provides a low-friction gliding surface for joint movement, and the cartilage damage and degeneration will cause inadequate lubrication on the joint surface [47,49,82]. Consequently, it is essential to reduce the frictional resistance between the implanted hydrogel scaffold and articular cartilage. As exhibited in Fig. S3, the coefficient of friction (COF) of Hydrogel-Exos maintained stable at approximately 0.04, which was much lower than that of porcine articular cartilage (0.11) reported by prior studies [83,84]. This low COF of Hydrogel-Exos can be attributed to the formation of hydration layer decreasing the frictional effect [47, 50,83]. Swelling is also a vital property of hydrogel scaffold in the application of cartilage tissue engineering [22]. As shown in Fig. S4, the Hydrogel-Exos reached the swelling equilibrium state after 72-h immersion in PBS. Additionally, the swelling ratio of Hydrogel-Exos was about 140 % (swelling equilibrium), suggesting that the size and cohesive adhesion of this hydrogel system remained stable in an underwater environment. Furthermore, although the adhesive strength of Hydrogel-Exos decreased after it reached swelling equilibrium, it still demonstrated superior adhesive strength than the fibrin glue (Figs. S6A and B).

Overall, our Hydrogel-Exos sustained release system was successfully constructed, demonstrating satisfactory gelation time, injectability, self-healing, frictional, swelling and mechanical properties with a porous texture, along with an extended exosome release capacity.

### 3.3. Adhesive performance of Hydrogel-Exos

Tissue adhesiveness plays a vital role in the application of adhesive hydrogel, requiring rapid and stable attachment to the target site while creating a favorable environment for cell growth and development [44]. To evaluate the adhesiveness of Hydrogel-Exos, fresh porcine cartilage pieces from the femoral condyles were prepared and subjected to lap-shear and end-to-end measurements (Fig. 3A and D). As depicted in Fig. 3B, C, E, and F, fibrin glue demonstrated the lowest adhesive strength ( $24.1 \pm 5.7$  kPa for lap-shear,  $12.89 \pm 5.74$  kPa for end-to-end), while the commercial cyanoacrylate adhesive ( $179.74 \pm 4.8$  kPa for lap-shear,  $183.72 \pm 2.65$  kPa for end-to-end) exhibited the highest adhesive strength before adhesion failure. Additionally, the adhesive strengths were significantly higher in the adhesive hydrogel ( $168.96 \pm 10.76$  kPa for lap-shear,  $154.50 \pm 7.21$  kPa for end-to-end) and Hydrogel-Exos ( $163.76 \pm 10.72$  kPa for lap-shear,  $145.51 \pm 4.47$  kPa for end-to-end) compared to fibrin glue, and comparable to the commercial cyanoacrylate adhesive. Notably, the Hydrogel-Exos successfully bonded two cartilage pieces on wooden blocks, demonstrating the capability to withstand a 500 g weight, even when submerged underwater (Fig. 3G). The robust tissue adhesion of adhesive hydrogels can be attributed to cohesion arising from their internal Schiff base reaction and hydrogen bonds, with interfacial adhesiveness resulting from Schiff base and hydrogen bonds between the hydrogel and the tissue [23]. Besides, these findings revealed that the embedding of exosomes did not influence the tissue adhesion of the adhesive hydrogel after the

hydrogen bond formation between the adhesive and exosomes. Moreover, the wetting resistance test for day 3 and 14 showed that the Hydrogel-Exos system could maintain stable in water over time (Fig. S5). Although the adhesive strength of soaked Hydrogel-Exos system decreased compared to its initial status, it still exhibited higher adhesive strength than the fibrin glue no matter on day 3 or day 14 (Figs. S6A and B).

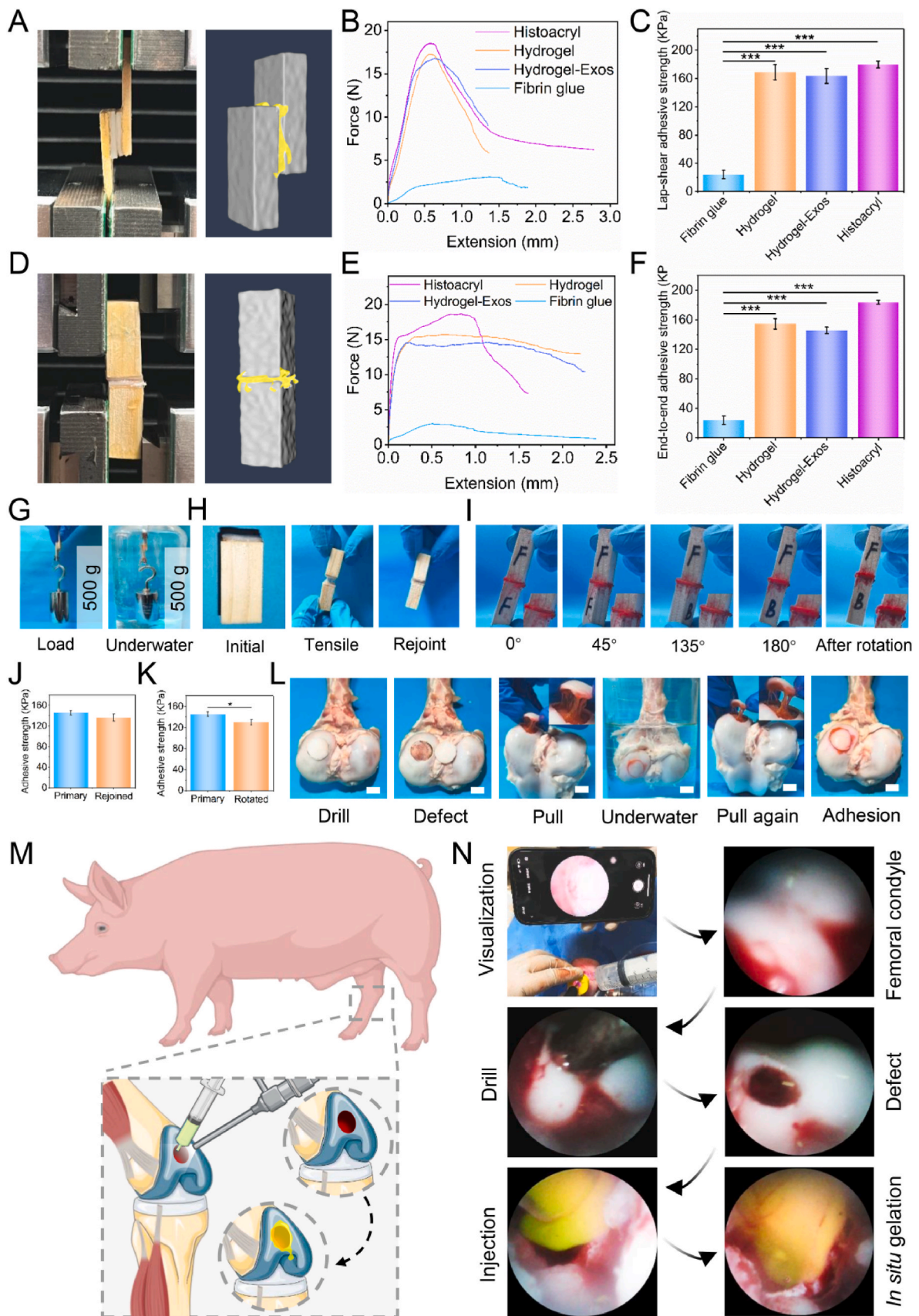
Apart from desirable adhesive strength, optimal flexibility is crucial in practical applications. Adjustable and flexible adhesion allows surgeons to readjust the adhesive hydrogel when injected into unwanted sites. As demonstrated in Fig. 3H, a pair of bonded cartilage pieces was broken and reconnected, with the rejoined pieces rapidly re-adhering after the self-healing of the Hydrogel-Exos. Furthermore, the adhesive strength of the rejoined pieces was measured again, revealing a non-significant decrease in strength (Fig. 3J). During another flexibility evaluation, one of the cartilage pieces was rotated by  $180^\circ$  (Fig. 3I). After rotation and self-healing, the adhesive strength was slightly reduced compared to the original pair (Fig. 3K). Furthermore, the Hydrogel-Exos successfully adhered to fresh porcine cartilage at the defect site after the cartilage piece was pulled, with or without underwater immersion (Fig. 3L). Such outstanding underwater adhesion ability of the adhesive hydrogel are derived from the Schiff base interaction between the aldehyde groups provided by OCS and the amino groups on wet tissue surface (Fig. S7) [23,85–88]. Moreover, the abundant hydrogen-bond interactions also contribute greatly to this remarkable underwater adhesion of the adhesive hydrogel (Fig. S7) [23, 85,88,89]. These findings collectively demonstrate that the Hydrogel-Exos possesses excellent rapid self-healing and reversible adhesion properties.

### 3.4. Evaluation of injection feasibility, *in situ* gelation, and wet tissue adhesiveness of adhesive under a water-filled arthroscopic environment in a swine model with knee cartilage defect

Having validated the adhesive hydrogel's rapid gelation, robust self-healing, smooth injectability, appropriate mechanical strength, and potent tissue adhesion, it appears to be well-suited for fluid-irrigated arthroscopic treatment. To assess its application feasibility, *in situ* gelation, and wet tissue adhesiveness at a cartilage defect, a swine model was established (Fig. 3M). A 7-mm-diameter, full-thickness, and cylindrical articular cartilage defect at the load-bearing region of the femoral condyle, known to lack the ability of self-healing [22], was employed. Continuous saline irrigation during the arthroscopic procedure is essential to expand the joint capsule and ensure adequate visualization [22]. As depicted in Fig. 3N, the adhesive hydrogel precursor was successfully injected into the chondral defect site. Consistent with the *ex vivo* assays, the adhesive hydrogel rapidly gelled and integrated well with the adjacent tissue, even in the water-irrigated joint cavity. Taken together, these findings suggest that the adhesive hydrogel serves as an appropriate scaffold for cartilage repair under saline-irrigated arthroscopic conditions, attributed to its rapid *in situ* gelation and high adhesiveness underwater. In recent years, minimally invasive arthroscopic procedures have become a prevalent option for the articular cartilage repair clinically, especially indicative for early and mid treatment [22]. Consequently, the adhesive hydrogel in this study may represent a significant and promising strategy in the clinical application.

### 3.5. *In vivo* hemostatic property of Hydrogel-Exos

It is widely acknowledged that hemophilic patients are prone to intraarticular bleeding upon damage to the articular cartilage, leading to hemosiderin deposits, the formation of a severe inflammatory micro-environment, hindering cartilage repair, and ultimately accelerating cartilage degeneration [6–9]. Therefore, an adhesive hydrogel with excellent hemostatic performance could be beneficial for enhanced cartilage repair. In this study, the hemostatic ability of Hydrogel-Exos



(caption on next page)

**Fig. 3.** Characterization of Hydrogel-Exos adhesive strength and reversible adhesiveness, and evaluation of injection feasibility of adhesive hydrogel at cartilage defect area under water-filled arthroscopic environment in a swine model. (A) Photographs and schematic diagrams showing the lap-shear Hydrogel-Exos adhesive strength test. (B–C) Representative stress-displacement curve and the adhesive strength of lap-shear tensile test. (D) Photographs and schematic diagrams showing the end-to-end Hydrogel-Exos strength test. (E–F) Representative stress-displacement curve and adhesive strength of end-to-end tensile test. (G) Photographs showing that the Hydrogel-Exos strongly adhered to two cartilage pieces on wooden blocks which could lift a weight of 500 g. (H) Reversible adhesiveness of Hydrogel-Exos was demonstrated by rejoining and reconnecting breaking cartilage pieces on wooden blocks. (I) Reversible adhesiveness of Hydrogel-Exos was demonstrated by rotating one of the bonded cartilage pieces for 180°. (J) The adhesive strength of rejoined cartilage pieces was tested again ( $n = 3$ ). (K) The adhesive strength of rotated cartilage pieces was tested again ( $n = 3$ ). (L) Hydrogel-Exos could adhere to fresh porcine cartilage at the defect site after the cartilage piece was pulled with or without underwater immersion. Scale bar: 5 mm. (M) Schematic illustration of adhesive hydrogel application in water-irrigated arthroscopic articular cartilage repair. (N) Images showing that the adhesive hydrogel could be successfully injected into the chondral defect site, formed rapidly, and integrated with the surrounding tissue, even in the saline-filled articular cavity. Statistical differences were determined by utilizing One-way ANOVA with Bonferroni's multiple comparison tests when comparing three or more groups. When comparing two groups, the unpaired  $t$ -test was utilized. (\* $P < 0.05$ , \*\* $P < 0.01$ , and \*\*\* $P < 0.001$ ).

was investigated using the liver hemorrhage, rat-tail amputation, and femoral condyle drill models on F8<sup>-/-</sup> rats [23,44,61,62]. In the liver hemorrhage model, the bloodstain area on the gauze gradually increased from 1 min to 3 min in the blank group but significantly decreased in the fibrin glue and Hydrogel-Exos groups (Figs. S8A and B). Moreover, the total blood loss in the non-treatment group ( $2.89 \pm 0.24$  g) was significantly higher than in the fibrin glue ( $1.3 \pm 0.16$  g) and Hydrogel-Exos groups ( $0.6 \pm 0.12$  g) (Fig. S8C). Additionally, treatment with fibrin glue ( $423.33 \pm 40.41$  s) and Hydrogel-Exos ( $243.33 \pm 25.17$  s) significantly reduced hemostatic time compared to the non-treatment group ( $556.67 \pm 40.41$  s) (Fig. S8D). It is widely acknowledged that the liver is a delicate organ with abundant microvascular networks and blood supply but lacks smooth-muscle contraction [90]. Accordingly, effectively controlling liver bleeding through conventional hemostatic approaches, such as cauterization or suturing, is challenging [90]. Accordingly, commercial fibrin glue represents an alternative for liver hemostasis and was selected for application in the treatment group in this study [23,90]. Notably, Hydrogel-Exos exhibited better liver hemostatic performance than fibrin glue, as verified by quantitative total blood loss and hemostatic time (Figs. S8C and D). This can be attributed to the wet tissue adhesiveness provided by Hydrogel-Exos and the formation of a physical barrier to reduce blood oozing [23,91]. Consistently, after rat-tail amputation, Hydrogel-Exos were associated with a reduction of more than 80 % and 60 % in total blood loss compared to the control and fibrin glue groups, respectively (Figs. S8E, F, and G). Additionally, the hemostasis time of the Hydrogel-Exos group ( $230 \pm 22.65$  s) was significantly shorter than the control ( $461.33 \pm 48.99$  s) and fibrin glue groups ( $363 \pm 28.83$  s) (Fig. S8H). Furthermore, Hydrogel-Exos adhered to and sealed the femoral condyle articular defect, significantly reducing hemorrhage from the marrow cavity (Figs. S8I and J). Importantly, both total blood loss and hemostasis time in this study exceeded previously reported data, possibly due to the coagulation disorders experienced by these rats after the knockout of F8 [23,62,91,92]. Nevertheless, these results highlight the outstanding *in vivo* hemostatic properties of Hydrogel-Exos. Besides, the Hydrogel-Exos system could contact with different shapes of cartilage defect, to further fill and seal the various bleeding sites (Fig. S9). It has been reported that gelatin, CS, and aldehyde groups in the adhesive hydrogel can promote blood clotting, enhance tissue adhesiveness, and provide an adhesive barrier sealing the bleeding site [23].

Unlike traditional ECM hydrogels, we found that the injectable Hydrogel-Exos system exhibited excellent wet tissue adhesion, thereby potentially addressing the challenge of recurrent intraarticular bleeding for patients with hemophilic articular cartilage damage under arthroscope.

### 3.6. Biocompatibility and migration of chondrocytes cultured on Hydrogel-Exos

It has been established that the cartilage tissue of the knee joint is mainly composed of hyaline cartilage, which includes chondrocytes and ECM. Hence, evaluating chondrocytes viability, proliferation, adhesion and migration after treatment with the Hydrogel-Exos is essential for the

repair of cartilage defect [40,52]. As shown by the live/dead staining, numerous cells survived (green fluorescence), and few cells died (red fluorescence) in each group, especially in the Hydrogel-Exos group (Fig. 4A and B). The CCK-8 results further revealed that the proliferation of chondrocytes increased with prolonged cultivation duration. In addition, on days 3 and 7, chondrocyte activity in the treatment group was significantly higher than the non-treated group, suggesting that the adhesive hydrogel and exosomes are beneficial for chondrocyte proliferation (Fig. 4C). Next, cytoskeleton imaging exhibited that chondrocytes were interconnected and stretched better on Hydrogel-Exos, compared to the other groups (Fig. 4D). After quantification, the spread area of the chondrocytes cultured on Hydrogel-Exos was the greatest among the four groups, indicating an excellent cell adhesion-promoting ability of adhesive and exosomes (Fig. 4E). It is widely acknowledged that chondrocyte migration is essential for the repair of cartilage defects [40,52]. Consequently, the effect of Hydrogel-Exos on chondrocyte migration was detected. The chondrocyte migration assay showed that the cells migrated significantly faster to the bare area on Hydrogel-Exos than on the other sample after 12 h and 24 h (Fig. 4F). Interestingly, chondrocytes accumulated at the denuded site in the Hydrogel-Exos group. Furthermore, quantitative analysis revealed that the 24-h denuded scratch area of the Hydrogel-Exos group ( $207.51 \pm 19.99 \times 10^3 \mu\text{m}^2$ ) was significantly lower than the control ( $481.98 \pm 36.28 \times 10^3 \mu\text{m}^2$ ), Hydrogel ( $315.11 \pm 20.20 \times 10^3 \mu\text{m}^2$ ) and Exos ( $305.17 \pm 30.45 \times 10^3 \mu\text{m}^2$ ) groups (Fig. 4G). The above findings substantiated that the Hydrogel-Exos scaffold is a viable candidate for promoting chondrocyte growth, adhesion, and migration. This positive outcome is likely due to the dual synergistic effect, wherein chondrocyte proliferation, regeneration, and migration are enhanced through the chondroitin sulfate provided by the adhesive and the exosomes released by the hydrogel network [1,2,18,26,27].

### 3.7. Biocompatibility of Hydrogel-Exos on RAW264.7 cells

Macrophages are known to abundantly infiltrate the hemophilic joint, particularly during the hemorrhagic active phase, exacerbating the inflammatory microenvironment and cartilage damage. Therefore, the biocompatibility of RAW264.7 cells on Hydrogel-Exos was also assessed [93–97]. Consistent with the chondrocyte results, both the live/dead and CCK-8 experiments demonstrated that Hydrogel-Exos exhibited excellent biocompatibility and stimulated viability in RAW264.7 cells (Figs. S10A, B, C). This favorable response can be attributed to BMSCs-derived exosomes enhancing cell proliferation and activity by inducing the phosphorylation of the AKT and ERK pathways [2,18,98].

### 3.8. Hydrogel-Exos facilitated M2 macrophage polarization

Considering the essential role of macrophages in regulating the inflammatory microenvironment and influencing the anabolic and catabolic balance of cartilage tissue, RAW264.7 cells were seeded on Hydrogel-Exos and cultured for 5 days to explore the immunomodulatory effects [2,4,15,18]. As depicted in Fig. 5A, macrophages can

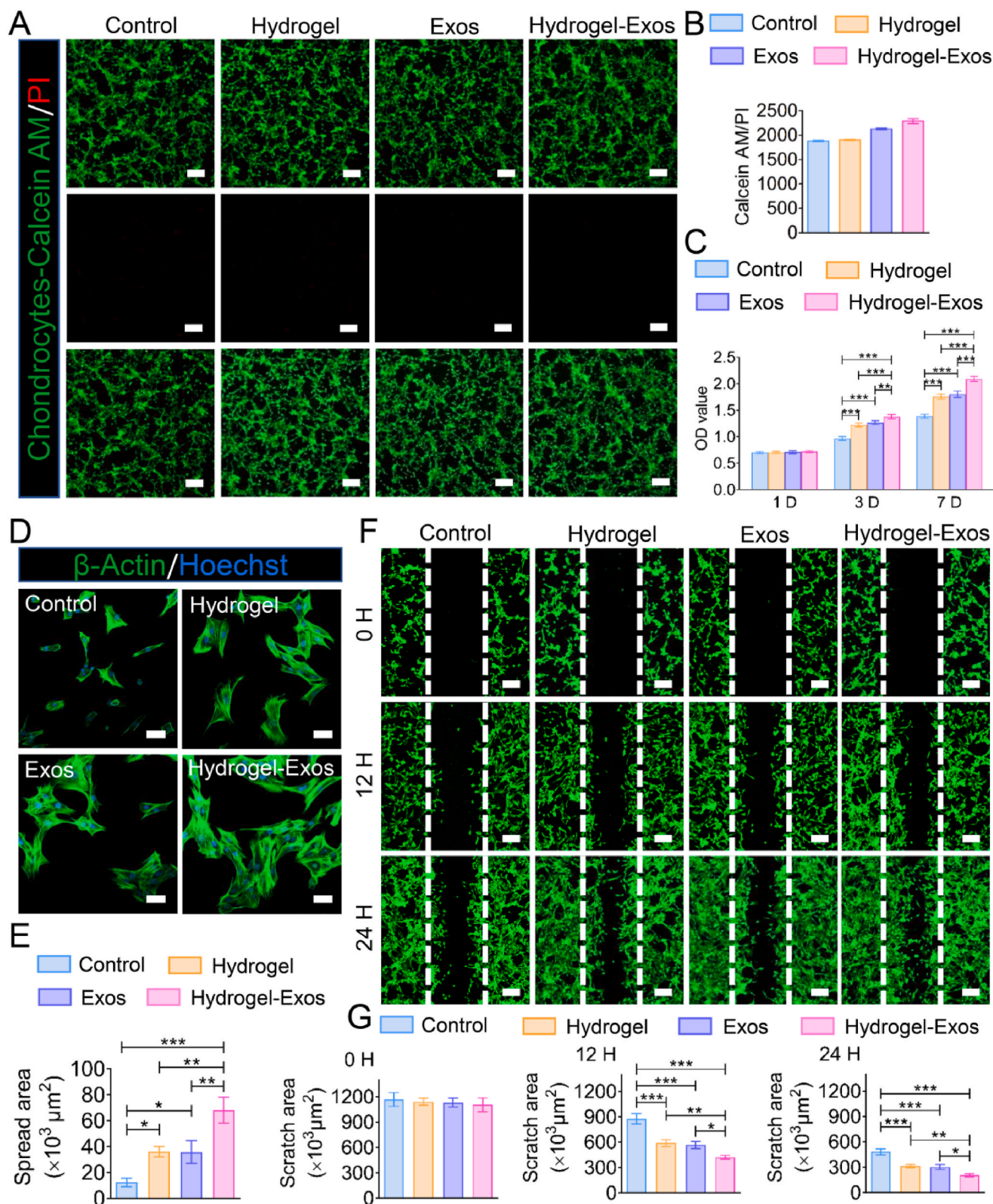
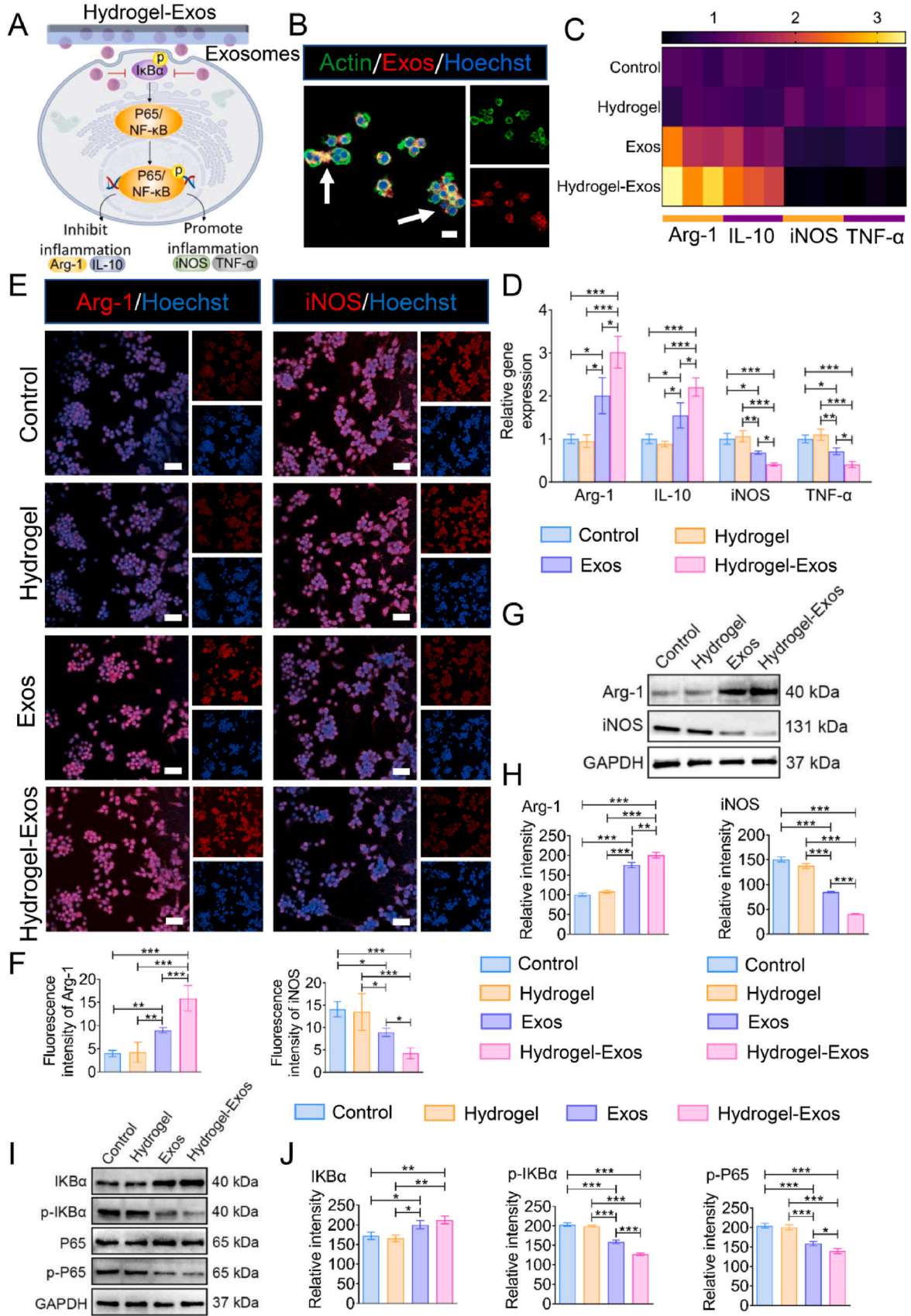


**Fig. 4.** Chondrocyte biocompatibility and migration on the Hydrogel-Exos. (A) Live/dead assay of the chondrocytes cultured on each sample surface for 1 day. Live cells were stained in green and dead cells in red. Scale bar: 200  $\mu$ m. (B) Quantification of live/dead assay (n = 3). (C) The CCK-8 assay of each sample was performed after 1, 3, and 7 days of cell culture (n = 3). (D) The cytoskeleton images showed the adhesion of chondrocytes after 3 days of culture on each group. Scale bar: 50  $\mu$ m. (E) Quantification of cell spread area (n = 5). (F) Wound-healing migration assay of the chondrocytes on each sample at different time points. Scale bar: 200  $\mu$ m. (G) Quantitative analysis of the scratch area at the denuded site at 0, 12, and 24 h (n = 3). Statistical differences were determined by utilizing One-way ANOVA with Bonferroni's multiple comparison tests when comparing three or more groups. When comparing two groups, the unpaired *t*-test was utilized. (\**P* < 0.05, \*\**P* < 0.01, and \*\*\**P* < 0.001).

utilized. (\* $P < 0.05$ , \*\* $P < 0.01$ , and \*\*\* $P < 0.001$ ).



(caption on next page)

**Fig. 5.** Hydrogel-Exos facilitated the polarization of RAW264.7 cells from M1 to M2 phenotype via the NF- $\kappa$ B pathway. (A) An illustration of Hydrogel-Exos modulating the macrophage polarization from an M1 to M2 phenotype. (B) Cytoskeleton staining imaging exhibited that PKH26-labeled exosomes released from the Hydrogel-Exos were endocytosed by RAW264.7 cells. Scale bar: 20  $\mu$ m. (C) Heat map showing the RT-qPCR results on the gene expressions of anti-inflammatory cytokines (Arg-1 and IL-10) and proinflammatory cytokines (iNOS and TNF- $\alpha$ ) in each group (n = 3). (D) Column graph showing the real-time qPCR (RT-qPCR) results on the gene expressions of anti-inflammatory cytokines (Arg-1 and IL-10) and proinflammatory cytokines (iNOS and TNF- $\alpha$ ) in each group (n = 3). (E) Immunofluorescence (IF) images displaying the amount of Arg-1 (red) positive and iNOS (red) positive RAW264.7 cells cultured on each group. Scale bar: 50  $\mu$ m. (F) Quantitative analysis of the fluorescence intensity of Arg-1 and iNOS (n = 3). (G) WB analysis of the Arg-1 and iNOS protein expression. (H) Protein band intensity of Arg-1 and iNOS was quantified utilizing ImageJ (n = 3). (I) WB analysis of the expression of the related proteins of the NF- $\kappa$ B pathway. (J) Quantification of the related proteins of NF- $\kappa$ B pathway (n = 3). Statistical differences were determined by utilizing One-way ANOVA with Bonferroni's multiple comparison tests when comparing three or more groups. When comparing two groups, the unpaired *t*-test was utilized. (\**P* < 0.05, \*\**P* < 0.01, and \*\*\**P* < 0.001).

differentiate into two phenotypes: M1 (pro-inflammatory) and M2 (anti-inflammatory) [2,4,15,18,98]. The M1 phenotype secretes pro-inflammatory cytokines such as tumor necrosis factor- $\alpha$  (TNF- $\alpha$ ) and inducible nitric oxide synthase (iNOS), contributing to an inflammatory response that hampers cartilage regeneration. Conversely, the M2 subgroup upregulates anti-inflammatory markers such as IL-10 and arginase-1 (Arg-1), promoting an anti-inflammatory environment that facilitates cartilage regeneration [4]. To induce severe inflammation and simulate hemophilic articular microenvironment, a relatively high concentration of lipopolysaccharide (LPS, 500 ng/ml) was added to pretreat RAW264.7 cells before each assay [18,99–104]. BMSCs-derived exosomes released from Hydrogel-Exos can be internalized by RAW264.7 cells, leveraging their immunoregulatory capacity (Fig. 5B). RT-qPCR results demonstrated that mRNA expressions of Arg-1 and IL-10 (anti-inflammatory markers) in RAW264.7 cells treated with exosomes and Hydrogel-Exos were significantly upregulated compared to those without exosome treatment. In contrast, gene levels of iNOS and TNF- $\alpha$  (pro-inflammatory cytokines) were significantly downregulated in the pure exosomes group and Hydrogel-Exos group compared to the other two groups (Fig. 5C and D). Additionally, IF assay results revealed that the abundance of Arg-1-labeled cells was significantly higher in both the exosomes-treated groups than in the control and pure adhesive groups, whereas the number of iNOS-labeled cells was significantly lower (Fig. 5E and F). Consistent with the qPCR and IF results, WB analysis further showed that exosomes and Hydrogel-Exos treatments significantly elevated the protein expression levels of Arg-1 but reduced the protein levels of iNOS (Fig. 5G and H). However, there was no significant difference between the pure adhesive group and control group in gene expression, IF staining, and WB analysis, suggesting that adhesive alone could not influence macrophage polarization (Fig. 5C, D, E, F, G, and H) [18]. Notably, the addition of exosomes into adhesive significantly upregulated the expressions of anti-inflammatory markers and downregulated the levels of pro-inflammatory cytokines compared to the treatment of exosomes alone, indicating that the sustained release of exosomes effectively facilitates long-term M2 macrophage polarization [18,32,33,98]. Taken together, these findings suggest that Hydrogel-Exos yield favorable immunomodulatory effects via regulating M2 macrophage polarization.

Moreover, to explore the potential mechanism of this immunoregulatory ability of Hydrogel-Exos, the protein levels in the NF- $\kappa$ B inflammatory pathway were assessed (Fig. 5I and J). Compared to the other treatment groups, the protein expression of phosphorylated I $\kappa$ B $\alpha$  (p-I $\kappa$ B $\alpha$ ) was significantly downregulated in the Hydrogel-Exos group (Fig. 5I and J). Phosphorylated I $\kappa$ B $\alpha$  is a key regulator of the NF- $\kappa$ B signaling pathway, positively modulating the expression of pro-inflammatory molecules [33,98]. Consistently, the protein level of p-P65, a downstream molecule of the inflammatory NF- $\kappa$ B pathway, was significantly inhibited in the Hydrogel-Exos group (Fig. 5I and J). These findings substantiate that Hydrogel-Exos can modulate macrophage polarization from M1 to M2 by suppressing the NF- $\kappa$ B pathway. It has been reported that BMSCs-derived exosomes contain substantial active molecules such as lipids, proteins, and miRNAs, especially miR-199a, which plays a critical role in regulating the native immune system by inhibiting factors in the NF- $\kappa$ B pathway [18,32,33,98].

### 3.9. Hydrogel-Exos protected against IL-1 $\beta$ -induced chondrocyte damage via ameliorating the immune microenvironment

To investigate the influence of the ameliorated immune microenvironment on damaged chondrocytes, a chondrocyte/RAW264.7 cells/sample co-culture system was established (Fig. 6A). As previously described, chondrocytes were induced injury by treatment with IL-1 $\beta$  (10 ng/ml) before 24 h of the following experiments [56]. After 5 days of culture, the regeneration of chondrocyte ECM was assessed by gene expression, IF, and WB analysis. RT-qPCR findings showed that the exosomes group and Hydrogel-Exos group significantly upregulated COL-2 and SOX-9 expression in damaged chondrocytes while suppressing the gene levels of MMP-13, implying that treatment with exosomes, especially sustained exosomes, could protect injured chondrocytes (Fig. 6B and C). Besides, IF revealed that the abundance of COL-2-positive chondrocytes was significantly higher, whereas the amount of MMP-13-positive chondrocytes was significantly less when treated with exosomes and Hydrogel-Exos rather than treated without exosomes (Fig. 6D and E). Notably, the anabolism of ECM was greatly inhibited while the catabolic metabolism of ECM was significantly enhanced after treated by IL-1 $\beta$ , leading to the shrunken morphology of chondrocytes in COL-2 staining image and the plump morphology of chondrocytes in MMP-13 staining image [56]. This adverse metabolism of ECM was improved after the treatment with exosomes and Hydrogel-Exos (Fig. 6D). Consistently, WB analysis further showed that exosomes and Hydrogel-Exos treatments significantly promoted the protein expressions of COL-2 and SOX-9 but reduced the protein expression of MMP-13 (Fig. 6F and G). As a well-acknowledged collagenous component of cartilage tissue, COL-2 plays an essential role in the process of chondrocyte development and maturation [105]. Another chondrogenic marker, SOX-9, has been recognized as a critical transcription factor in cartilage repair due to its ability to modulate the expression of COL-2 and the synthesis of glycosaminoglycans [18]. In contrast, COL-2 and GAG can be degraded by MMP-13, a catabolic matrix metalloproteinase commonly expressed by damaged chondrocytes [2,105]. Overwhelming release of pro-inflammatory cytokines by M1 macrophages, such as TNF- $\alpha$  and IL-1 $\beta$ , can inhibit the expression of COL-2 and GAG by downregulating SOX9 and upregulating MMP-13 gene expression [2,9,18,105]. The results revealed that treatment with exosomes could attenuate the inhibitory effect of the inflammatory microenvironment on chondrocytes by promoting M2 macrophage polarization, thereby enhancing the production of cartilage ECM. However, there was no significant difference in the expression levels of COL-2, SOX-9, and MMP-13 between the pure adhesive group and the non-treated group (Fig. 6B, C, D, E, F, and G), indicating that treatment with adhesive alone could not mitigate the adverse effect of the inflammatory microenvironment on chondrocytes, attributing to its inability to modulate macrophage polarization. Furthermore, to verify the critical role of RAW264.7 cells in the immunomodulatory process, WB analysis was conducted after Hydrogel-Exos/chondrocytes were co-cultured with or without RAW264.7 cells for 5 days. The findings demonstrated that the chondrogenesis effect of Hydrogel-Exos was significantly weakened in the absence of RAW264.7 cells (Fig. 6H and I), suggesting that Hydrogel-Exos could yield desirable chondrogenic capacity through immunomodulation on macrophages. Taken together,

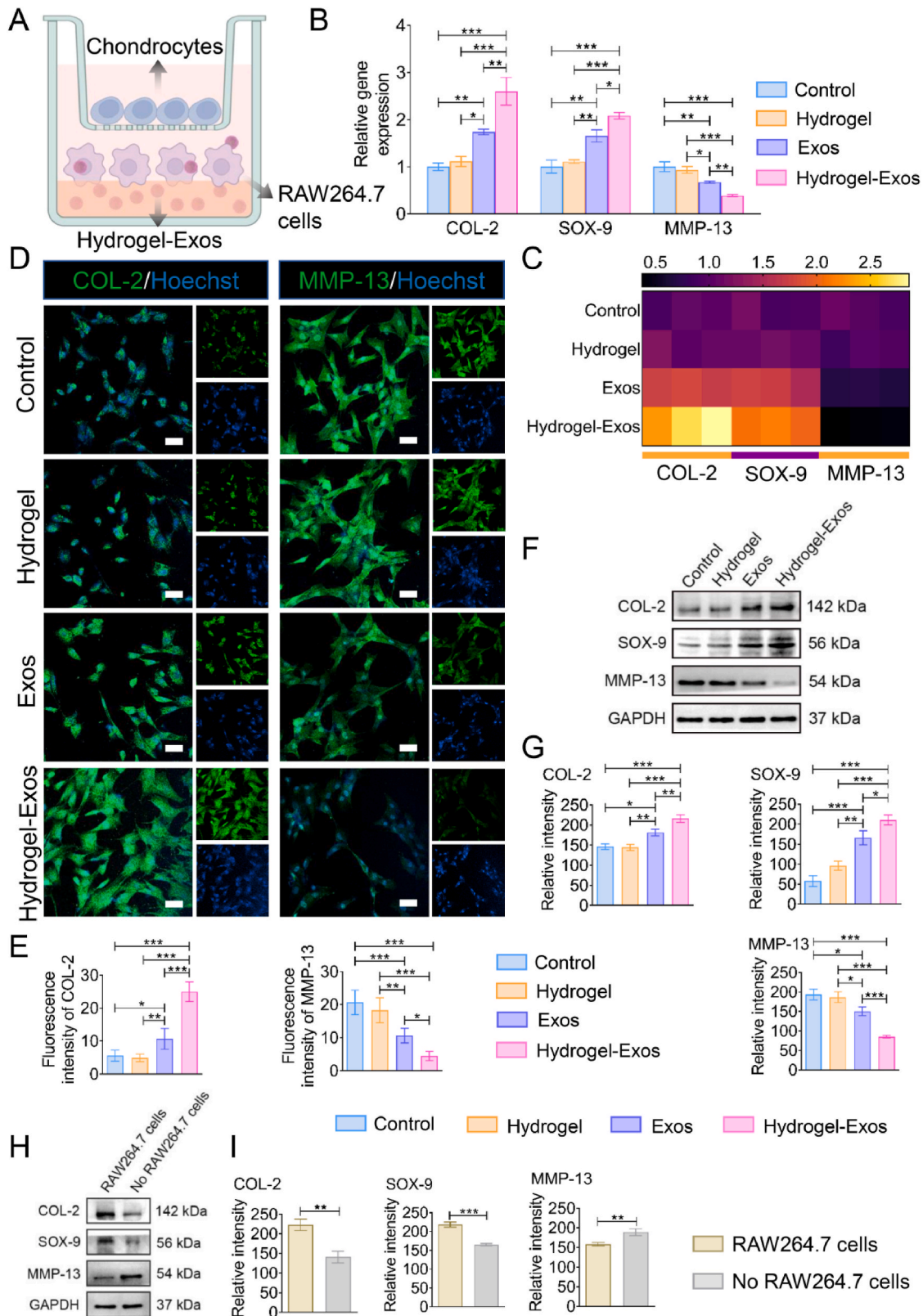


**Fig. 6.** Hydrogel-Exos protected against IL-1 $\beta$ -induced chondrocyte damage via ameliorating the immune microenvironment. (A) Construction of a co-culture model of damaged chondrocyte/RAW264.7 cells/sample. (B) Column graph showing the RT-qPCR results of COL-2, SOX-9 and MMP-13 (n = 3). (C) Heat map showing the RT-qPCR results of COL-2, SOX-9 and MMP-13 (n = 3). (D) IF images displaying the amount of COL-2 (green) positive and MMP-13 (green) positive chondrocytes cultured on each group. Scale bar: 50  $\mu$ m. (E) Quantitative analysis of the fluorescence intensity of COL-2 and MMP-13 (n = 3). (F) WB analysis of the COL-2, SOX-9 and MMP-13 protein expression. (G) Quantitative analysis of the COL-2, SOX-9 and MMP-13 protein expression (n = 3). (H–I) WB assay and quantitative analysis after 5 days of Hydrogel-Exos/chondrocyte co-culture with or without RAW 264.7 cells (n = 3). Statistical differences were determined by utilizing One-way ANOVA with Bonferroni's multiple comparison tests when comparing three or more groups. When comparing two groups, the unpaired *t*-test was utilized. (\**P* < 0.05, \*\**P* < 0.01, and \*\*\**P* < 0.001).

Hydrogel-Exos could exert an excellent chondrogenesis effect by inhibiting the inflammatory microenvironment.

### 3.10. Hydrogel-Exos directly alleviated IL-1 $\beta$ -induced chondrocyte damage

To further assess the direct chondrogenic capacity of Hydrogel-Exos, IL-1 $\beta$ -pretreated chondrocytes were cultured directly on each sample in the absence of RAW264.7 cells for 5 days (Fig. 7A). As shown in the cytoskeleton staining results, the exosomes released from Hydrogel-Exos could be endocytosed by chondrocytes after 24 h (Fig. 7B). The RT-qPCR, IF, and WB results exhibited that the expression of chondrogenic genes or proteins, including COL-2 and SOX-9 in the pure adhesive group, was significantly elevated compared to the control group, while the catabolic factor MMP-13 was significantly reduced (Fig. 7C, D, E, F, G, and H), suggesting that treatment with adhesive alone can directly contribute to the alleviation of chondrocyte damage. Chondroitin sulfate, the main component of adhesive, has been reported to promote the expression of TGF- $\beta$ 1 through binding to integrins, leading to the increased synthesis of COL-2 and hyaluronic acid, thereby stimulating cartilage regeneration [1,18,26,27,106]. In addition, the genes and protein levels of COL-2 and SOX-9 in the exosomes group and Hydrogel-Exos group demonstrated significant upregulation compared to the control group, but the level of MMP-13 presented contrasting results, specifically in the Hydrogel-Exos group (Fig. 7C, D, E, F, G, and H). This finding indicated that exosomes could attenuate IL-1 $\beta$ -induced chondrocyte damage, and when loaded on adhesive, they could further enhance the protective effect of injured chondrocytes. It has been proven that exosomes can secrete non-coding RNAs, such as miR-92a and miR-23b, to regulate chondrogenesis and cartilage matrix production via the MAPK, ERK, and AKT signaling pathways [2,18,107]. The above data revealed that Hydrogel-Exos could yield satisfactory protective performance for chondrocytes through the dual direct chondrogenesis effect from adhesive hydrogel and the lastingly released exosomes. Therefore, Hydrogel-Exos could provide a synergistically favorable microenvironment for chondrogenesis via the immunoregulatory and direct chondroprotective effects.

### 3.11. *In vivo* exosome delivery capacity and biodegradation of Hydrogel-Exos

In addition to the evaluation of *in vitro* exosome release, the *in vivo* exosome retention in Hydrogel-Exos was investigated via bioluminescence imaging technology. As observed in Fig. 8A, B, C, and D, PKH26-labeled exosomes delivered in PBS were only detectable within 3 days after the initial injection into the cartilage defect site, while those loaded on the adhesive hydrogel were still detectable on day 14, further substantiating that Hydrogel-Exos yielded outstanding performance for sustained release of exosomes both *in vitro* and *in vivo*. As mentioned earlier, this prolonged delivery capacity of Hydrogel-Exos can be due to the formation of reversible hydrogen bonds between exosomes and adhesive hydrogel [18,23,32,33]. Additionally, bioluminescence imaging showed that the application of Hydrogel-Exos system allowed the released exosomes to work locally around the cartilage defect in the knee joint (Fig. 8A and C). Next, *in vivo* biodegradation was investigated using an *in vivo* imaging system after subcutaneous implantation of Cy7-labeled Hydrogel-Exos into the dorsum of rats. The imaging results showed an extended duration of the fluorescence signal, which decreased slowly for 21 days (Fig. 8E and F). In addition, tissue samples were harvested for macroscopic observation and histological analysis at different time points. As shown in Fig. 8G, there were no significant signs of inflammatory reactions, such as redness or swelling, throughout the whole process. Besides, the adhesive bulk decreases gradually with a small volume of residual on day 21, suggesting that Hydrogel-Exos was slowly degraded *in vivo* (Fig. 8G). The quantitative rate of *in vivo* degradation of hydrogels revealed that the Hydrogel-Exos could be

degraded about 90 % within 3 weeks (Figs. S11A and B). H&E staining further verified that there was no obvious tissue response, and the adhesive hydrogel can be gradually degraded (Fig. 8H). It is universally recognized that biopolymers such as gelatin and CS in Hydrogel-Exos can be naturally biodegraded by intrinsic enzymes, including collagenase, chondroitinase, or hyaluronidase [23]. This degradation cycle is generally aligned with the repair timeline of the cartilage tissue. It is well acknowledged that the initial period required for cartilage repair is 4 weeks, which indicated that the hydrogel scaffolds should be gradually degraded within 4 weeks [1,15,55,99,108]. Given that slow degradation of hydrogels cannot match well with the regeneration progress of cartilage and the residual hydrogels can further impede the integration of neocartilage, the Hydrogel-Exos system in this study demonstrated an appropriate degradation cycle for cartilage repair [1,108]. Importantly, this degradation profile was consistent with the exosomes release, allowing the sustained delivery of exosomes and CS, and thereby providing favorable environment for hemophilic cartilage repair. These findings demonstrated that Hydrogel-Exos had desirable biodegradability and slow degradation characteristics, which provided sufficient time for cartilage repair [23,43,44].

### 3.12. *In vivo* biocompatibility of Hydrogel-Exos

It is well-established that the biocompatibility of biomaterials is essential for their *in vivo* application in the field of tissue engineering [99]. Given the local application of natural ECM hydrogel and the limited existence of vascular tissue within the joint, the possibility of systemic dissemination and toxicity was minimized [109]. Nevertheless, in addition to the *in vitro* biocompatibility evaluation, there are a considerable number of studies further assessing the *in vivo* biocompatibility of foreign biomaterials in cartilage tissue engineering, which may be due to that degradation products of polymer hydrogels can be metabolized through vital organs [1,99,109–111]. Therefore, before implementing Hydrogel-Exos for the treatment of hemophilic articular cartilage defects, we conducted *in vivo* biocompatibility assessments. These evaluations encompassed hemocompatibility studies, including hemolysis tests and serum protein examinations, as well as histopathological examinations of major organs such as the heart, lungs, liver, spleen, and kidneys. The hemolytic test is widely recognized as a crucial measure for assessing the hemocompatibility of foreign materials [32,33,51]. As depicted in Fig. S12A, serum extracted from foreign biomaterials (adhesive hydrogel, exosomes, and Hydrogel-Exos) co-incubated whole blood exhibited a reddish color, similar to the negative control group (PBS). In contrast, the positive control group (Triton-100X) displayed a carmine color. The serum OD values of the biomaterial groups were comparable to the PBS group and significantly different from the Triton-100X group (Fig. S12B). The hemolytic ratio for the biomaterial groups was consistently below 1.0 %, indicating exceptional hemocompatibility of Hydrogel-Exos. Additionally, the levels of ALT, AST, and TP (common serum proteins) in the three treated groups were comparable to those in the control groups, suggesting the absence of systemic toxicity resulting from Hydrogel-Exos (Fig. S12C). Furthermore, histopathological examination (H&E staining) confirmed the absence of apparent pathological alterations in major organs harvested from rats treated with adhesives. No significant deposition of degradation products from the adhesive hydrogels was observed (Fig. S12D). In summary, the results above substantiate the *in vitro* and *in vivo* biocompatibility of Hydrogel-Exos, supporting its suitability for treating hemophilic articular cartilage defects [23].

### 3.13. Hydrogel-Exos relieved pain and restored joint function after hemophilic knee joint cartilage defect

To further assess whether Hydrogel-Exos treatment can relieve pain and restore joint function after hemophilic knee joint cartilage defect, pain measurements and gait analysis were performed. PWT and TWL

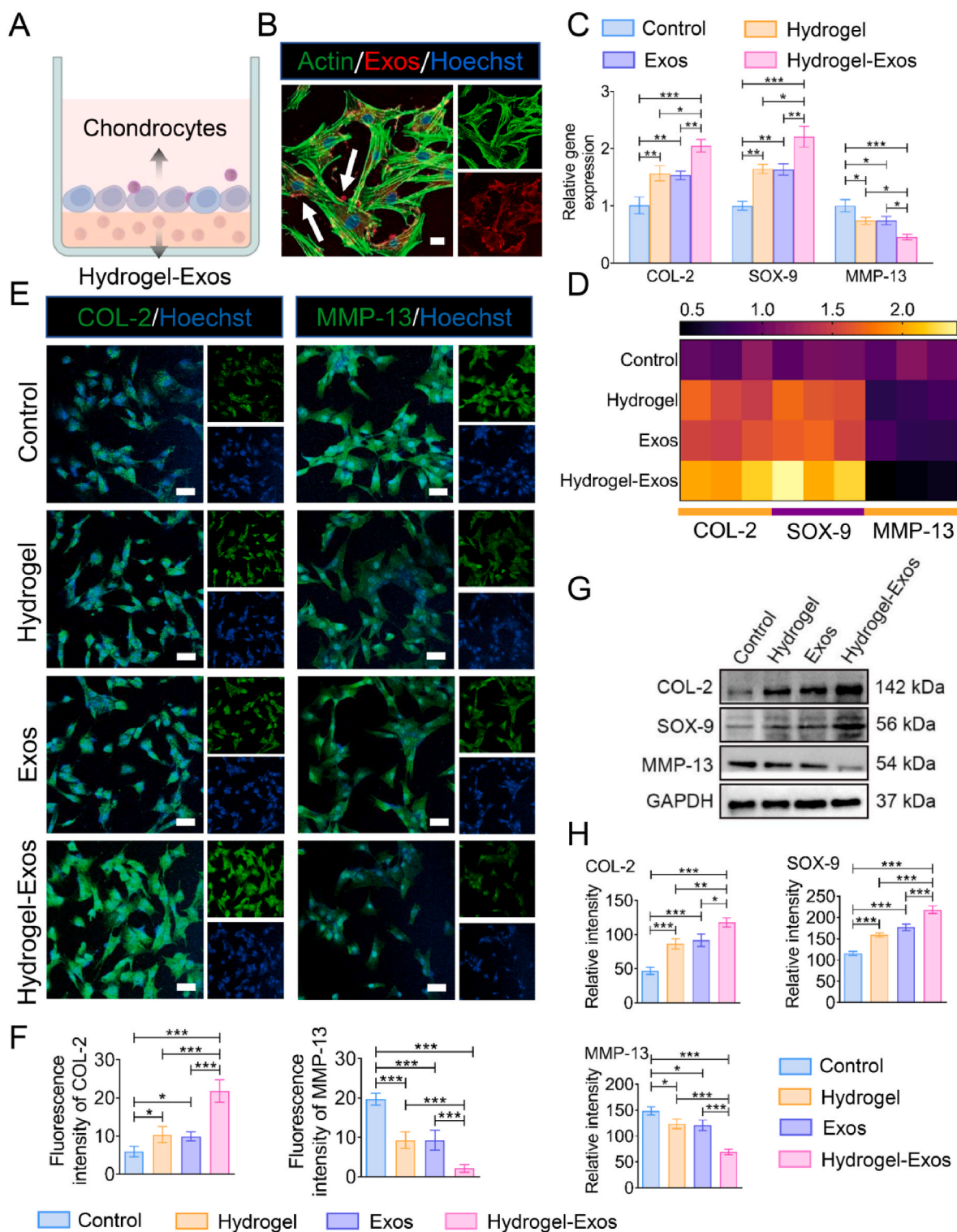


**Fig. 7.** Hydrogel-Exos directly promote the repair of damaged chondrocytes. (A) Construction of a co-culture model of damaged chondrocytes/samples. (B) Cytoskeleton staining imaging exhibited that PKH26-labeled exosomes released from the Hydrogel-Exos were endocytosed by chondrocytes. Scale bar: 50  $\mu$ m. (C) Column graph showing the RT-qPCR results of COL-2, SOX-9, and MMP-13 (n = 3). (D) Heat map showing the RT-qPCR results of COL-2, SOX-9, and MMP-13 (n = 3). (E) IF images displaying the amount of COL-2 (green) positive and MMP-13 (green) positive chondrocytes cultured on each group. Scale bar: 50  $\mu$ m. (F) Quantitative analysis of the fluorescence intensity of COL-2 and MMP-13 (n = 3). (G) WB analysis of the COL-2, SOX-9, and MMP-13 protein expression. (H) Quantitative analysis of the COL-2, SOX-9, and MMP-13 protein expression (n = 3). Statistical differences were determined by utilizing One-way ANOVA with Bonferroni's multiple comparison tests when comparing three or more groups. When comparing two groups, the unpaired *t*-test was utilized. (\**P* < 0.05, \*\**P* < 0.01, and \*\*\**P* < 0.001).

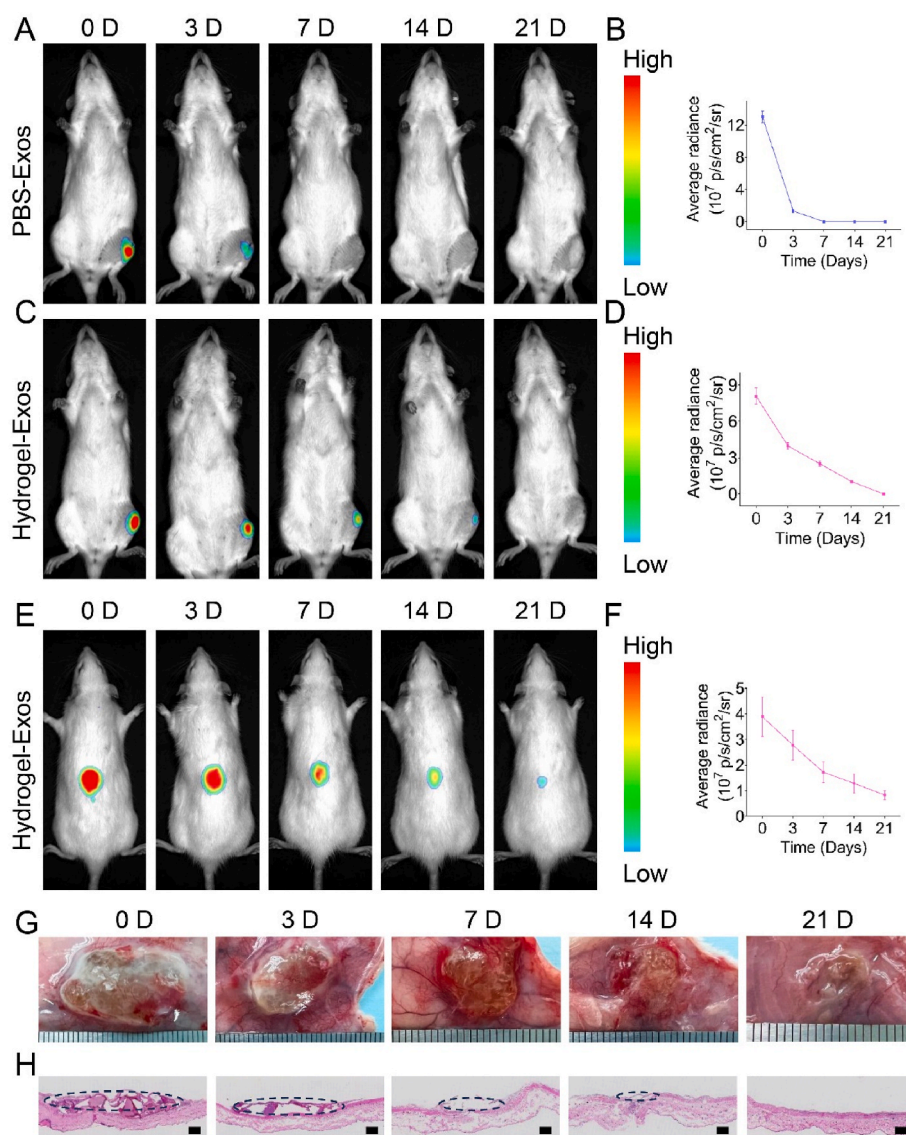


**Fig. 8.** *In vivo* exosomes delivery capacity and biodegradation of Hydrogel-Exos. (A–B) PKH26-labeled exosomes delivered in PBS ( $n = 3$ ). (C–D) PKH26-labeled exosomes loaded on the adhesive hydrogel. (E–F) The imaging results showed an extended duration of fluorescence signal which was decreased slowly for 21 days ( $n = 3$ ). (G) Gross observation of subcutaneous degradation of Hydrogel-Exos ( $n = 3$ ). (H) Hematoxylin-eosin (H&E) staining further verified that there was no obvious tissue response after 21 days and the adhesive hydrogel can be gradually degraded ( $n = 3$ ). Scale bar: 1 mm. Statistical differences were determined by utilizing One-way ANOVA with Bonferroni's multiple comparison tests when comparing three or more groups. When comparing two groups, the unpaired *t*-test was utilized. (\* $P < 0.05$ , \*\* $P < 0.01$ , and \*\*\* $P < 0.001$ ).

were used to evaluate the mechanical allodynia and thermal sensitivity, respectively (Fig. 9A and D) [56–58]. As exhibited in Fig. 9B and C, after knee joint cartilage injury, the PWT values were significantly reduced from baseline in rats treated with adhesive hydrogel, exosomes or without treatment. Although the PWT also decreased from baseline in the Hydrogel-Exos group, it was significantly greater than the other three groups for 6 weeks after surgery, implying animals in this group experienced less pain (Fig. 9B and C). Consistently, the TWL in rats treated with Hydrogel-Exos was significantly longer compared to the other treatment groups, suggesting these rats suffered hypoalgesia (Fig. 9E and F). Notably, the PWT and TWL in the exosomes group were greater than that in adhesive hydrogel and untreated groups only in the first week, which indicated that the monotherapy of exosomes could achieve pain easement after cartilage damage, but their *in vivo* rapid release limited the sustained pain relief to a large extent (Fig. 9B, C, E and F). Interestingly, the PWT and TWL in the adhesive hydrogel group were greater than in the untreated group after 4 weeks of treatment,

illustrating that adhesive hydrogel partially repaired hemophilic cartilage defect and thus slightly relieved pain (Fig. 9B, C, E and F). Importantly, the loading of exosomes in adhesive hydrogel obviously extended the anti-inflammatory effect of exosomes in the early stage and greatly repaired cartilage defect in the middle and late stages to yield satisfactory pain relief throughout the whole process (Fig. 9B, C, E and F).

After verifying the effect of pain relief on hemophilic knee joint cartilage injury, we further assessed the ability of Hydrogel-Exos to improve limb function by gait analysis. Ranging from –100 (complete function loss) to 0 (normal function), SFI is a widely-used index to evaluate the restoration of limb motor function, and calculated by determining three footprint parameters as shown in Fig. 9G [51,59,60]. The deficit of limb motor function after nerve, muscle or joint damage can alter footprint parameters, such as a decrease in the TS and ITS while an increase in the PL. In a representative footprint measurement after 6 weeks of knee joint cartilage injury, the untreated and pure exosomes groups exhibited dragged footprints with a reduction of TS and ITS and

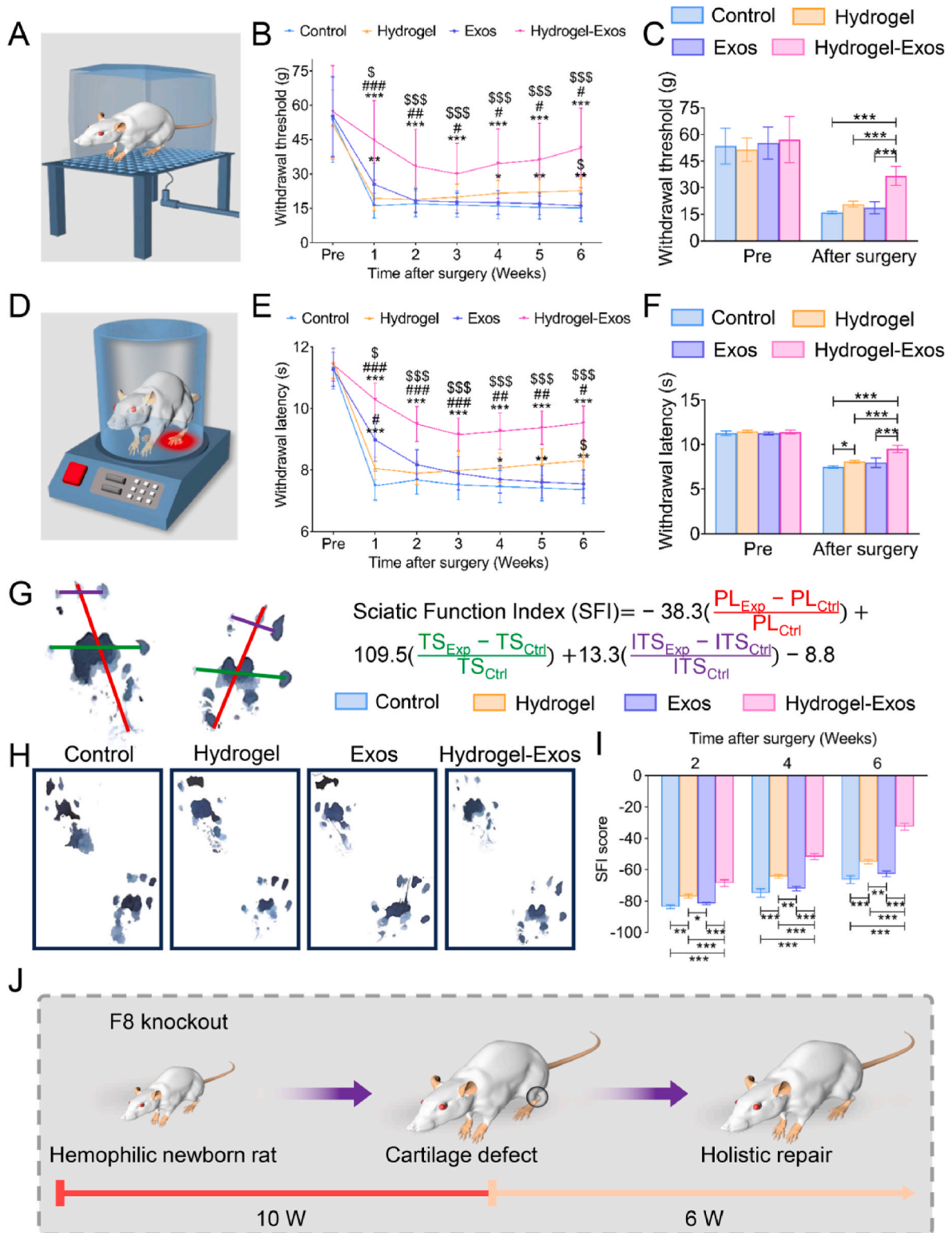


**Fig. 9.** Hydrogel-Exos relieved pain and restored joint function after hemophilic knee joint cartilage defect. (A) Schematic diagram illustrating the mechanical allodynia experiment with von-Frey filaments. (B) Alterations of paw withdrawal threshold (PWT) in each group after hemophilic knee joint cartilage defect compared to baseline (before model construction) (n = 4). (C) Average PWT of each group before and after the procedure (n = 4). (D) Schematic diagram illustrating the thermal sensitivity response by hot plate experiment. (E) Alterations of thermal withdrawal latency (TWL) in each group after hemophilic knee joint cartilage defect compared to baseline (before model construction) (n = 4). (F) Average TWL of each group before and after the procedure (n = 4). (G) The equation for calculating the SFI according to three footprint parameters. (H) Representative photographs of the footprints among groups. (I) Sciatic function index (SFI) scores of different treatment groups 2, 4, and 6 weeks after the operation (n = 3). (J) Illustration depicting the establishment and repair process of hemophilic knee joint cartilage defect. Statistical differences were determined by utilizing One-way ANOVA with Bonferroni's multiple comparison tests when comparing three or more groups. When comparing two groups, the unpaired *t*-test was utilized. (\**P* < 0.05, \*\**P* < 0.01, and \*\*\**P* < 0.001).

an increment of PL, whereas the Hydrogel-Exos group showed clear footprints with an increment of TS and ITS and a reduction of PL (Fig. 9H). In comparison to the untreated group (SFI =  $-66.36 \pm 2.52$ ), adhesive hydrogel group (SFI =  $-54.94 \pm 1.32$ ) and exosomes group (SFI =  $-62.59 \pm 1.72$ ), limb function in the Hydrogel-Exos group (SFI =  $-32.58 \pm 2.18$ ) improved significantly after 6 weeks of treatment (Fig. 9I). Rats with monotherapy of adhesive hydrogel presented a moderate footprints result (Fig. 9H and I). Overall, although the capacity of pain relief and joint function recovery in the exosomes group was

inferior to the adhesive hydrogel group in the later stage, the encapsulation of exosomes in adhesive hydrogel can synergistically improve joint function via the dual effect of early anti-inflammation and long-lasting chondrogenesis after hemophilic knee joint cartilage defect.

### 3.14. Hydrogel-Exos promoted cartilage repair in a hemophilic knee joint cartilage defect model

A full-thickness knee joint cartilage defect model was established in

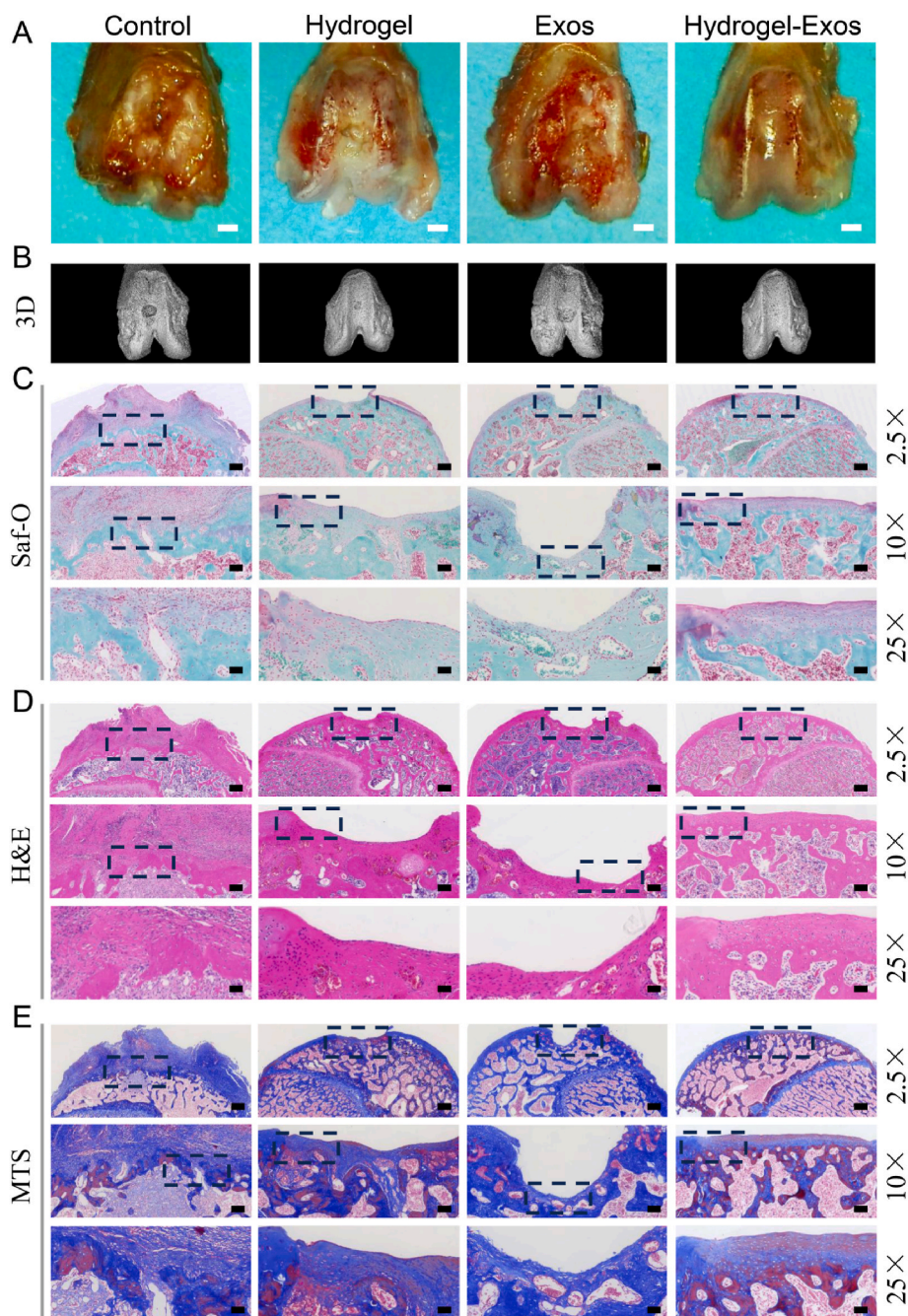


**Fig. 10.** Hydrogel-Exos promoted cartilage repair in a hemophilic knee joint cartilage defect model. (A) Gross observation of knee cartilage repair at 6 weeks after treatment. Scale bar: 1 mm. (B) Top (3D) views of micro-CT examinations from the repaired hemophilic articular cartilage. (C) Safranin-O/fast green (Saf-O) staining of femoral condyles harvested from hemophilic rats to observe the effect of cartilage repair 6 weeks after the Hydrogel-Exos injection. Scale bar: 500  $\mu$ m (at low magnification), 125  $\mu$ m (at moderate magnification), and 50  $\mu$ m (at high magnification). (D) H&E staining of femoral condyles harvested from hemophilic rats to observe the effect of cartilage repair 6 weeks after the Hydrogel-Exos injection. Scale bar: 500  $\mu$ m (at low magnification), 125  $\mu$ m (at moderate magnification), and 50  $\mu$ m (at high magnification). (E) Masson trichrome staining (MTS) of femoral condyles harvested from hemophilic rats to observe the effect of cartilage repair 6 weeks after the Hydrogel-Exos injection. Scale bar: 500  $\mu$ m (at low magnification), 125  $\mu$ m (at moderate magnification), and 50  $\mu$ m (at high magnification).

hemophilic rats to assess the *in vivo* chondral regeneration capability of Hydrogel-Exos. Notably, the results of Perl's Prussian Blue staining showed that there was substantial deposition of hemosiderin in hemophilic articular cartilage defect lesion (Fig. S13). Following 6 weeks of treatment, both gross observations and histological assessments were conducted at the target site. As depicted in Fig. 10A, the Hydrogel-Exos treated group exhibited clearly regenerated cartilage-like tissues that seamlessly integrated with neighboring cartilage tissue. In contrast, the untreated and pure exosomes groups displayed rough surfaces and deep concavities. Additionally, the monotherapy of adhesive hydrogel showed moderate results with minimal neo-tissue and partial cartilage repair (Fig. 10A). Given that subchondral bone plays an essential role in bearing weight, structural support, and articular cartilage regeneration, the quality of subchondral bone was assessed by micro-CT examinations and 3D reconstruction. As observed in Fig. 10B and Fig. S14A, substantial neo-bones fully filled the defect in the Hydrogel-Exos group, whereas few neo-bones and obvious cavity were found in the untreated and pure exosomes groups. After quantification, the Hydrogel-Exos treated group exhibited the highest BV/TV, Tb.N and Tb.Th values and the lowest Tb.Sp value among the four groups (Fig. S14B). Consistent with the gross observation, the treatment of adhesive hydrogel alone presented moderate subchondral bone formation (Fig. 10B and Fig. S14).

Consistent findings were observed in Saf-O, H&E, and MTS staining, indicating that defect regions in the untreated and pure exosomes groups were filled with neo-fibrous granulation tissue, and no newly formed cartilage tissue was observed (Fig. 10C, D, and E). Conversely, the Hydrogel-Exos treated group displayed defect areas covered with a smooth and thick cartilage layer containing abundant glycosaminoglycans, with no clear boundary between the regenerated and surrounding host cartilage (Fig. 10C, D, and E). In the pure adhesive hydrogel group, defects were partially repaired, suggesting that the provision of ECM components could yield a moderate effect on chondral repair (Fig. 10C, D, and E). Importantly, the loading of exosomes in adhesive hydrogel demonstrated satisfactory cartilage regeneration, attributed to the sustained release of exosomes and slow degradation of the adhesive hydrogel. As previously described, both chondroitin sulfate and exosomes in this Hydrogel-Exos composite play roles in stimulating chondrogenesis and cartilage matrix production [1,2,18,26,27,106,107].

### 3.15. Hydrogel-Exos modulated *in vivo* immune microenvironment and increased the production of cartilage matrix after hemophilic cartilage defect

To investigate whether Hydrogel-Exos can mitigate the *in vivo* inflammatory microenvironment following hemophilic cartilage defects, we conducted an immunohistochemistry analysis to assess the expression of iNOS at the injury site. As depicted in Fig. 11A and D, there was no significant difference in iNOS expression among the untreated, adhesive hydrogel, and exosomes groups, suggesting that treatment with hydrogel alone or the rapid release of exosomes was insufficient in regulating the local inflammatory microenvironment at the defect site. In contrast, the expression of iNOS in the Hydrogel-Exos group was significantly lower compared to the other three groups (Fig. 11A and D), potentially attributable to the prolonged release of exosomes, which exerted a sustained anti-inflammatory effect. The inflammatory microenvironment plays a critical role in cartilage repair, as excessive pro-inflammatory cytokines such as iNOS, IL-1 $\beta$ , and TNF- $\alpha$  can lead to overexpression of MMP-13, exacerbating chondrocyte damage and ECM degradation following cartilage injury, especially in patients with hemophilia [9,18,95,112]. Therefore, suppressing the inflammatory microenvironment after hemophilic cartilage defects is beneficial for ECM production and chondrocyte survival.

Furthermore, we evaluated the expression of COL-2 and MMP-13 at the repair site through immunohistochemistry analysis. Adhesive treatment alone significantly increased COL-2 expression while reducing

MMP-13 expression compared to the non-treated and pure exosomes groups (Fig. 11B, C, E, and F), suggesting that the adhesive hydrogel can enhance chondrocyte anabolism and inhibit catabolism through direct supplementation of ECM [1,18,26,27]. Importantly, the Hydrogel-Exos group exhibited significantly upregulated COL-2 expression and downregulated MMP-13 expression compared to the other groups (Fig. 11B, C, E, and F), indicating that the sustained release of exosomes in conjunction with adhesive hydrogel achieved synergistic cartilage repair for hemophilic cartilage damage [1,2,18,26,27,106,107]. However, exosome monotherapy did not influence the expression of COL-2 and MMP-13 (Fig. 11B, C, E, and F), suggesting that the rapid release of exosomes alone may not effectively exert their chondrogenic and immunoregulatory effects in long-term cartilage repair [14,19,20,34]. Collectively, these results confirm that Hydrogel-Exos enhances the repair of hemophilic cartilage defects through anti-inflammation and direct cartilage regeneration.

In summary, our *in vivo* studies revealed that treatment with adhesive hydrogel alone exhibited superior efficacy in repairing cartilage defects in rats with hemophilia compared to exosome monotherapy. Accordingly, the application of exosomes alone may not ensure sustained release and effective retention at the target site, thereby failing to meet the demands of cartilage repair. In contrast, the adhesive hydrogel, known for its slow *in vivo* degradation and ability to provide ECM components continuously, demonstrated effective cartilage repair [1,18,26,27]. Interestingly, the encapsulation of exosomes in adhesive hydrogel via reversible noncovalent bonding significantly enhanced the reparability. The synergy between exosomes and adhesive hydrogel promoted cartilage regeneration through immunoregulation and direct chondrogenesis (Fig. 1). Additionally, the favorable hemostasis performance of Hydrogel-Exos created a beneficial microenvironment for hemophilic cartilage repair by reducing hemosiderin deposits, inhibiting the inflammatory microenvironment, and preventing cartilage degeneration [6–9].

Based on the inspiration from the work by Guan et al., this study used partial similar verification methods to assess the treatment effect of Hydrogel-Exos system [18]. However, there are three major differences between this study and the previous research reported by Guan et al. First, their animal model is growth plate injury in normal rats with a moderate inflammatory microenvironment, while the animal model in the present study is articular cartilage defect in hemophilic (F8<sup>-/-</sup>) rats with a severer inflammatory microenvironment (Fig. 9J). Consequently, anti-inflammatory treatment and immune regulation would be more beneficial and meaningful for hemophilic articular cartilage defect. Additionally, their therapeutic system is ordinary ECM hydrogel without desirable adhesion, whereas the adhesive hydrogel in this study with outstanding wet tissue adhesion in harsh joint cavity, allowing the local sustained delivery of exosomes in the damaged area to synergistically yield satisfactory treatment for hemophilic articular cartilage defect. Moreover, this innovative approach is well-suited for application during arthroscopic procedures verified in a swine cartilage defect model, offering a promising strategy for addressing the complex challenges associated with hemophilic articular cartilage damage. Therefore, we believe that our study is innovative in the field of tissue engineering for holistic repair of hemophilic articular cartilage defect.

## 4. Conclusion

In conclusion, we successfully developed an injectable hydrogel adhesive loaded with exosomes, presenting a remarkable ability to address early intra-articular bleeding, modulate the inflammatory microenvironment in the initial stages, and promote chondrogenesis throughout the entire process for hemophilic cartilage defects. The adhesive hydrogel was created by blending OCS and gelatin in the presence of borax. The exosomes derived from BMSCs were then loaded onto the hydrogel adhesive through the formation of reversible noncovalent hydrogen bonds, ensuring their prolonged release and concentration at

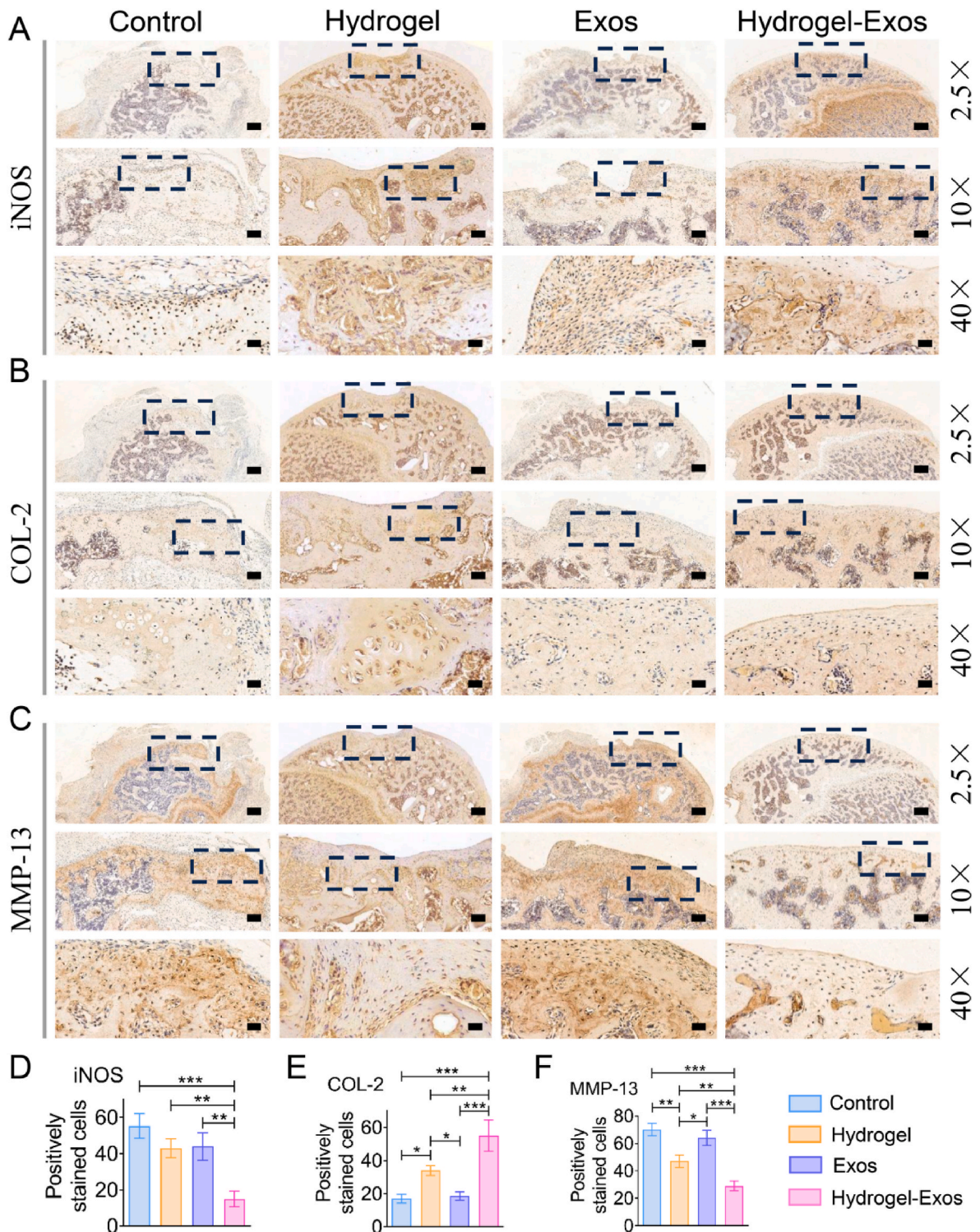


**Fig. 11.** Hydrogel-Exos modulated *in vivo* immune microenvironment and increased the production of cartilage matrix after hemophilic cartilage defect. (A) Immunohistochemistry for iNOS expression in the defect area at 6 weeks after treatment. Scale bar: 500 μm (at low magnification), 125 μm (at moderate magnification), and 40 μm (at high magnification). (B) Immunohistochemistry for COL-2 expression in the defect area at 6 weeks after treatment. Scale bar: 500 μm (at low magnification), 125 μm (at moderate magnification), and 40 μm (at high magnification). (C) Immunohistochemistry for MMP-13 expression in the defect area at 6 weeks after treatment. Scale bar: 500 μm (at low magnification), 125 μm (at moderate magnification), and 40 μm (at high magnification). (D–F) The quantitative analysis of positively stained cells for iNOS, COL-2, and MMP-13 in samples. Statistical differences were determined by utilizing One-way ANOVA with Bonferroni’s multiple comparison tests when comparing three or more groups. When comparing two groups, the unpaired *t*-test was utilized. (\**P* < 0.05, \*\**P* < 0.01, and \*\*\**P* < 0.001).

the target site to meet the therapeutic requirements for long-term cartilage repair. Beyond its excellent injectability, self-healing ability, and wet tissue adhesiveness stemming from dynamic Schiff base bonds and hydrogen bonds, the Hydrogel-Exos composite exhibited satisfactory biocompatibility, biodegradability, swelling process, COF, mechanical properties, and hemostatic performance. Moreover, our adhesive hydrogel demonstrated successful injection into the knee joint cartilage defect region and *in situ* gelation under the water-filled arthroscopic environment in a swine model. Additionally, through *in vitro* and *in vivo* assays, we confirmed that Hydrogel-Exos could inhibit the inflammatory microenvironment by regulating macrophage M2 polarization via the NF- $\kappa$ B pathway. This improved inflammatory microenvironment, in turn, protected damaged chondrocytes and promoted extracellular matrix anabolism. Furthermore, both *in vitro* and *in vivo* validations demonstrated that Hydrogel-Exos could directly enhance chondrogenesis by providing ECM components and allowing the sustained release of chondrogenic and anti-inflammatory exosomes, facilitating the cartilage repair and joint function restoration after hemophilic articular cartilage defects. In summary, our Hydrogel-Exos system represents a promising therapeutic strategy for reducing early intra-articular bleeding, improving the inflammatory microenvironment, and fostering long-term chondrogenesis in the context of hemophilic cartilage defects. The system is well-suited for arthroscopic applications.

### Funding

This work was supported by the National Natural Science Foundation of China Youth Fund (82202662), the Guangzhou Science and Technology Program (2023A04J2314), the National Natural Science Foundation of China (12,272,164), the China Postdoctoral Science Foundation (2023M741563), the Clinical Research Startup Program of Southern Medical University by High-level University Construction Funding of Guangdong Provincial Department of Education (LC2019ZD001), the Clinical Research Program of Nanfang Hospital, Southern Medical University (2019CR016), the Project of Drug Clinical Evaluate Research of Chinese Pharmaceutical Association (CPA-Z06-ZC-2021-004), the National Natural Science Foundation of China (82370497), the Medical Scientific Research Foundation of Guangdong (A2024366), Huizhou Science Technology Project Foundation (2022CZ010423), the Macau Science and Technology Development fund (FDCT (0012/2021/AMJ, 003/2022/ALC, 0092/2022/A2,0144/2022/A3)), the Shenzhen-Hong Kong-Macao Science and Technology Fund (Category C: SGDX20220530111203020), the Foundation of Guangdong Basic and Applied Basic Research Foundation (2022A1515140151&2022A1515140189&2023A1515140045&2022-A1515140071), and the National Orthopaedics Key Clinical Specialty Construction Research Foundation of Huizhou Central People's Hospital.

### Ethics approval and consent to participate

All animal studies were conducted in strict accordance with the guidelines outlined in the National Institutes of Health Guide for the Care and Use of Laboratory Animals. The research protocols were comprehensively reviewed and approved by the Animal Experimental Ethics Committee of Southern Medical University Nanfang Hospital.

### CRedit authorship contribution statement

**Qinfeng Yang:** Writing – original draft, Validation, Methodology, Investigation, Formal analysis, Conceptualization. **Guihua Liu:** Methodology, Investigation. **Guanghao Chen:** Methodology, Formal analysis. **Guo Chen:** Validation, Investigation, Funding acquisition, Formal analysis. **Keyu Chen:** Validation, Formal analysis. **Lei Fan:** Visualization, Resources, Funding acquisition, Data curation. **Yuesheng Tu:**

Validation, Methodology. **Jialan Chen:** Visualization, Investigation. **Zhanjun Shi:** Visualization, Resources. **Chuan Chen:** Validation, Methodology, Formal analysis. **Shubo Liu:** Validation, Formal analysis. **Geyang Deng:** Investigation, Formal analysis. **Xiaoqian Deng:** Validation, Software. **Chunhan Sun:** Visualization, Formal analysis. **Xiaoyang Li:** Visualization, Resources. **Shuofei Yang:** Supervision, Resources. **Shaowei Zheng:** Supervision, Resources, Funding acquisition. **Bin Chen:** Supervision, Methodology, Funding acquisition.

### Declaration of competing interest

The authors declare that they have no known competing financial interests or personal relationships that could have appeared to influence the work reported in this paper.

### Acknowledgments

We thank Lei Fan and Yian Luo for their help in drawing the schematic diagram and typesetting figures.

### Appendix A. Supplementary data

Supplementary data to this article can be found online at <https://doi.org/10.1016/j.bioactmat.2024.08.018>.

### References

- [1] F.X. Zhang, P. Liu, W. Ding, Q.B. Meng, D.H. Su, Q.C. Zhang, R.X. Lian, B.Q. Yu, M.D. Zhao, J. Dong, Y.L. Li, L.B. Jiang, Injectable Mussel-Inspired highly adhesive hydrogel with exosomes for endogenous cell recruitment and cartilage defect regeneration, *Biomaterials* 278 (2021) 121169, <https://doi.org/10.1016/j.biomaterials.2021.121169>.
- [2] S. Zhang, S.J. Chuah, R.C. Lai, J.H.P. Hui, S.K. Lim, W.S. Toh, MSC exosomes mediate cartilage repair by enhancing proliferation, attenuating apoptosis and modulating immune reactivity, *Biomaterials* 156 (2018) 16–27, <https://doi.org/10.1016/j.biomaterials.2017.11.028>.
- [3] M. Li, H. Yin, Z. Yan, H. Li, J. Wu, Y. Wang, F. Wei, G. Tian, C. Ning, H. Li, C. Gao, L. Fu, S. Jiang, M. Chen, X. Sui, S. Liu, Z. Chen, Q. Guo, The immune microenvironment in cartilage injury and repair, *Acta Biomater.* 140 (2022) 23–42, <https://doi.org/10.1016/j.actbio.2021.12.006>.
- [4] J. Zeng, L. Huang, H. Xiong, Q. Li, C. Wu, Y. Huang, H. Xie, B. Shen, Injectable decellularized cartilage matrix hydrogel encapsulating urine-derived stem cells for immunomodulatory and cartilage defect regeneration, *Npj Regen. Med.* 7 (2022) 1–12, <https://doi.org/10.1038/s41536-022-00269-w>.
- [5] Y. Peng, Y. Zhuang, Y. Liu, H. Le, D. Li, M. Zhang, K. Liu, Y. Zhang, J. Zuo, J. Ding, Bioinspired gradient scaffolds for osteochondral tissue engineering, *Explorations* 3 (2023), <https://doi.org/10.1002/EXP.20210043>.
- [6] R. Buda, M. Cavallo, F. Castagnini, A. Cenacchi, S. Natali, F. Vannini, S. Giannini, Treatment of hemophilic ankle arthropathy with one-step arthroscopic bone marrow-derived cells transplantation, *Cartilage* 6 (2015) 150–155, <https://doi.org/10.1177/1947603515574286>.
- [7] R. Ravanbod, G. Torkaman, M. Mophid, F. Mohammadali, Experimental study on the role of intra-articular injection of MSCs on cartilage regeneration in haemophilia, *Haemophilia* 21 (2015) 693–701, <https://doi.org/10.1111/hae.12659>.
- [8] Y. Sogi, Y. Yabe, Y. Hagiwara, M. Tsuchiya, Y. Onoda, T. Sekiguchi, N. Itaya, S. Yoshida, T. Yano, K. Suzuki, T. Onoki, E. Itoi, Joint hemorrhage accelerates cartilage degeneration in a rat immobilized knee model, *BMC Musculoskel. Disord.* 21 (2020) 1–12, <https://doi.org/10.1186/s12891-020-03795-0>.
- [9] L. Zheng, Z. Han, D. Luo, J. Li, H. Ye, R. Feng, Q. Zhong, J. Jing, Y. Yao, FGF23 and SOX9 expression in haemophilic cartilage: *in vitro* studies of the effects of iron, *Haemophilia* 28 (2022) 1062–1068, <https://doi.org/10.1111/hae.14623>.
- [10] L. Zheng, Z. Han, D. Luo, J. Li, N. Pang, M. Ding, H. Ye, K. Zhu, Y. Yao, IL-6, IL-1 $\beta$  and TNF- $\alpha$  regulation of the chondrocyte phenotype: a possible mechanism of haemophilic cartilage destruction, *Hematologia* 28 (2023), <https://doi.org/10.1080/16078454.2023.2179867>.
- [11] N. Wagener, S. Hardt, M. Pumberger, F. Schömg, Cartilage destruction by hemophilic arthropathy can be prevented by inhibition of the ferroptosis pathway in human chondrocytes, *J. Clin. Med.* 13 (2024), <https://doi.org/10.3390/jcm13020559>.
- [12] L. Nieuwenhuizen, R.E.G. Schutgens, B.S. van Asbeck, M.J. Wenting, K. van Veghel, G. Roosendaal, D.H. Biesma, F.P.J.G. Lafeber, Identification and expression of iron regulators in human synovium: evidence for upregulation in haemophilic arthropathy compared to rheumatoid arthritis, osteoarthritis, and healthy controls, *Haemophilia* 19 (2013) 218–227, <https://doi.org/10.1111/hae.12208>.
- [13] A.J. Lee, L.R. Gangi, F. Zandkarimi, B.R. Stockwell, C.T. Hung, Red blood cell exposure increases chondrocyte susceptibility to oxidative stress following

- hemarthrosis, *Osteoarthritis, What Car?* 31 (2023) 1365–1376, <https://doi.org/10.1016/j.joca.2023.06.007>.
- [14] X. Liu, Y. Yang, Y. Li, X. Niu, B. Zhao, Y. Wang, C. Bao, Z. Xie, Q. Lin, L. Zhu, Integration of stem cell-derived exosomes with in situ hydrogel glue as a promising tissue patch for articular cartilage regeneration, *Nanoscale* 9 (2017) 4430–4438, <https://doi.org/10.1039/c7nr00352h>.
- [15] D. Gan, Y. Jiang, Y. Hu, X. Wang, Q. Wang, K. Wang, C. Xie, L. Han, X. Lu, Mussel-inspired extracellular matrix-mimicking hydrogel scaffold with high cell affinity and immunomodulation ability for growth factor-free cartilage regeneration, *J. Orthop. Transl.* 33 (2022) 120–131, <https://doi.org/10.1016/j.jot.2022.02.006>.
- [16] E. Stocco, S. Barbon, P. Radossi, S. Rajendran, D. Dalzoppo, M. Bortolami, A. Bagnò, F. Grandi, P.G. Gamba, P.P. Parnigotto, G. Tagariello, C. Grandi, Autologous chondrocytes as a novel source for neo-chondrogenesis in haemophilias, *Cell Tissue Res.* 366 (2016) 51–61, <https://doi.org/10.1007/s00441-016-2408-8>.
- [17] Y. Peng, Y. Zhuang, Y. Zhang, J. Zuo, J. Ding, Dynamically adaptive scaffolds for cartilage tissue engineering, *MedComm - Biomater. Appl.* 2 (2023) 1–12, <https://doi.org/10.1002/mba2.49>.
- [18] P. Guan, C. Liu, D. Xie, S. Mao, Y. Ji, Y. Lin, Z. Chen, Q. Wang, L. Fan, Y. Sun, Exosome-loaded extracellular matrix-mimic hydrogel with anti-inflammatory property facilitates/promotes growth plate injury repair, *Bioact. Mater.* 10 (2022) 145–158, <https://doi.org/10.1016/j.bioactmat.2021.09.010>.
- [19] D. Deng, X. Li, J.J. Zhang, Y. Yin, Y. Tian, D. Gan, R. Wu, J. Wang, B.M. Tian, F. M. Chen, X.T. He, Biotin-avidin system-based delivery enhances the therapeutic performance of MSC-derived exosomes, *ACS Nano* 17 (2023) 8530–8550, <https://doi.org/10.1021/acsnano.3c00839>.
- [20] J. Zeng, P. Sun, Y. Zhao, X. Fang, Z. Wu, X. Qi, Bone mesenchymal stem cell-derived exosomes involved co-delivery and synergism effect with icariin via mussel-inspired multifunctional hydrogel for cartilage protection, *Asian J. Pharm. Sci.* 18 (2023) 100799, <https://doi.org/10.1016/j.ajps.2023.100799>.
- [21] Q. Wang, J. Luan, Z. Zhao, W. Kong, C. Zhang, J. Ding, Dentin-desensitizing biomaterials, *Chin. Chem. Lett.* 34 (2023) 108060, <https://doi.org/10.1016/j.ccl.2022.108060>.
- [22] Y. Hua, H. Xia, L. Jia, J. Zhao, D. Zhao, X. Yan, Y. Zhang, S. Tang, G. Zhou, L. Zhu, Q. Lin, Ultrafast, tough, and adhesive hydrogel based on hybrid photocrosslinking for articular cartilage repair in water-filled arthroscopy, *Sci. Adv.* 7 (2021), <https://doi.org/10.1126/sciadv.abg0628>.
- [23] L. Zhou, C. Dai, L. Fan, Y. Jiang, C. Liu, Z. Zhou, P. Guan, Y. Tian, J. Xing, X. Li, Y. Luo, P. Yu, C. Ning, G. Tan, Injectable self-healing natural biopolymer-based hydrogel adhesive with thermoresponsive reversible adhesion for minimally invasive surgery, *Adv. Funct. Mater.* 31 (2021) 1–13, <https://doi.org/10.1002/adfm.202007457>.
- [24] K. Han, Q. Bai, W. Wu, N. Sun, N. Cui, T. Lu, Gelatin-based adhesive hydrogel with self-healing, hemostasis, and electrical conductivity, *Int. J. Biol. Macromol.* 183 (2021) 2142–2151, <https://doi.org/10.1016/j.ijbiomac.2021.05.147>.
- [25] J. Huang, Z. Huang, Y. Liang, W. Yuan, L. Bian, L. Duan, Z. Rong, J. Xiong, D. Wang, J. Xia, 3D printed gelatin/hydroxyapatite scaffolds for stem cell chondrogenic differentiation and articular cartilage repair, *Biomater. Sci.* 9 (2021) 2620–2630, <https://doi.org/10.1039/d0bm02103b>.
- [26] J. Shin, E.H. Kang, S. Choi, E.J. Jeon, J.H. Cho, D. Kang, H. Lee, I.S. Yun, S. W. Cho, Tissue-adhesive chondroitin sulfate hydrogel for cartilage reconstruction, *ACS Biomater. Sci. Eng.* 7 (2021) 4230–4243, <https://doi.org/10.1021/acsbomaterials.0c01414>.
- [27] J. Zhang, B. Li, J. Zuo, R. Gu, B. Liu, C. Ma, J. Li, K. Liu, An engineered protein adhesive with properties of tissue integration and controlled release for efficient cartilage repair, *Adv. Healthcare Mater.* 10 (2021) 1–7, <https://doi.org/10.1002/adhm.202100109>.
- [28] E.C. Rodriguez-Merchan, Intra-articular injections of mesenchymal stem cells (MSCs) as a treatment for hemophilic arthropathy, *Expert Rev. Hematol.* 9 (2016) 737–741, <https://doi.org/10.1080/17474086.2016.1203780>.
- [29] X. Sang, X. Zhao, L. Yan, X. Jin, X. Wang, J. Wang, Z. Yin, Y. Zhang, Z. Meng, Thermosensitive hydrogel loaded with primary chondrocyte-derived exosomes promotes cartilage repair by regulating macrophage polarization in osteoarthritis, *Tissue Eng. Regen. Med.* 19 (2022) 629–642, <https://doi.org/10.1007/s13770-022-00437-5>.
- [30] L. Wang, F. Li, L. Wang, B. Wu, M. Du, H. Xing, S. Pan, Exosomes derived from bone marrow mesenchymal stem cells alleviate rheumatoid arthritis symptoms via shuttling proteins, *J. Proteome Res.* (2023), <https://doi.org/10.1021/acs.jproteome.3c00697>.
- [31] J. Zhou, Z. Zhang, J. Joseph, X. Zhang, B.E. Ferdows, D.N. Patel, W. Chen, G. Banfi, R. Molinaro, D. Cosco, N. Kong, N. Joshi, O.C. Farokhzad, C. Corbo, W. Tao, Biomaterials and nanomedicine for bone regeneration: progress and future prospects, *Explorations* 1 (2021), <https://doi.org/10.1002/EXP.20210011>.
- [32] L. Fan, C. Liu, X. Chen, L. Zheng, Y. Zou, H. Wen, P. Guan, F. Lu, Y. Luo, G. Tan, P. Yu, D. Chen, C. Deng, Y. Sun, L. Zhou, C. Ning, Exosomes-loaded electroconductive hydrogel synergistically promotes tissue repair after spinal cord injury via immunoregulation and enhancement of myelinated axon growth, *Adv. Sci.* 9 (2022) 1–22, <https://doi.org/10.1002/advs.202105586>.
- [33] Q. Yang, S. Su, S. Liu, S. Yang, J. Xu, Y. Zhong, Y. Yang, L. Tian, Z. Tan, J. Wang, Z. Yu, Z. Shi, F. Liang, Exosomes-loaded electroconductive nerve dressing for nerve regeneration and pain relief against diabetic peripheral nerve injury, *Bioact. Mater.* 26 (2023) 194–215, <https://doi.org/10.1016/j.bioactmat.2023.02.024>.
- [34] H. Cao, M. Chen, X. Cui, Y. Liu, Y. Liu, S. Deng, T. Yuan, Y. Fan, Q. Wang, X. Zhang, Cell-free osteoarthritis treatment with sustained-release of chondrocyte-targeting exosomes from umbilical cord-derived mesenchymal stem cells to rejuvenate aging chondrocytes, *ACS Nano* 17 (2023) 13358–13376, <https://doi.org/10.1021/acsnano.3c01612>.
- [35] Z. Wang, H. Le, Y. Wang, H. Liu, Z. Li, X. Yang, C. Wang, J. Ding, X. Chen, Instructive cartilage regeneration modalities with advanced therapeutic implantations under abnormal conditions, *Bioact. Mater.* 11 (2022) 317–338, <https://doi.org/10.1016/j.bioactmat.2021.10.002>.
- [36] Z. Li, M. Li, P. Xu, J. Ma, R. Zhang, Compositional variation and functional mechanism of exosomes in the articular microenvironment in knee osteoarthritis, *Cell Transplant.* 29 (2020) 1–10, <https://doi.org/10.1177/0963689720968495>.
- [37] Z. Ni, S. Zhou, S. Li, L. Kuang, H. Chen, X. Luo, J. Ouyang, M. He, X. Du, L. Chen, Exosomes: roles and therapeutic potential in osteoarthritis, *Bone Res* 8 (2020), <https://doi.org/10.1038/s41413-020-0100-9>.
- [38] Q. Liu, R. Wang, S. Hou, F. He, Y. Ma, T. Ye, S. Yu, H. Chen, H. Wang, M. Zhang, Chondrocyte-derived exosomes promote cartilage calcification in temporomandibular joint osteoarthritis, *Arthritis Res. Ther.* 24 (2022) 1–16, <https://doi.org/10.1186/s13075-022-02738-5>.
- [39] F. Li, Z. Xu, Z. Xie, X. Sun, C. Li, Y. Chen, J. Xu, G. Pi, Adipose mesenchymal stem cells-derived exosomes alleviate osteoarthritis by transporting microRNA -376c-3p and targeting the WNT-beta-catenin signaling axis, *Apoptosis* 28 (2023) 362–378, <https://doi.org/10.1007/s10495-022-01787-0>.
- [40] S. Li, J. Liu, S. Liu, W. Jiao, X. Wang, Chitosan oligosaccharides packaged into rat adipose mesenchymal stem cells-derived extracellular vesicles facilitating cartilage injury repair and alleviating osteoarthritis, *J. Nanobiotechnol.* 19 (2021) 1–19, <https://doi.org/10.1186/s12951-021-01086-x>.
- [41] L. Yin, Y. Wu, Z. Yang, V. Denzlin, X. Ren, C.A. Tee, Z. Lai, C.T. Lim, J. Han, E. H. Lee, Characterization and application of size-sorted zonal chondrocytes for articular cartilage regeneration, *Biomaterials* 165 (2018) 66–78, <https://doi.org/10.1016/j.biomaterials.2018.02.050>.
- [42] L. Zhou, L. Fan, F.-M. Zhang, Y. Jiang, M. Cai, C. Dai, Y.-A. Luo, L.-J. Tu, Z.-N. Zhou, X.-J. Li, C.-Y. Ning, K. Zheng, A.R. Boccacini, G.-X. Tan, Hybrid gelatin/oxidized chondroitin sulfate hydrogels incorporating bioactive glass nanoparticles with enhanced mechanical properties, mineralization, and osteogenic differentiation, *Bioact. Mater.* 6 (2021) 890–904, <https://doi.org/10.1016/j.bioactmat.2020.09.012>.
- [43] Y. Yang, S. Su, S. Liu, W. Liu, Q. Yang, L. Tian, Z. Tan, L. Fan, B. Yu, J. Wang, Y. Hu, Triple-functional bone adhesive with enhanced internal fixation, bacteriostasis and osteoinductive properties for open fracture repair, *Bioact. Mater.* 25 (2023) 273–290, <https://doi.org/10.1016/j.bioactmat.2023.01.021>.
- [44] C. Liu, W. Liu, B. Qi, L. Fan, S. Liu, Q. Yang, Y. Yang, S. Yang, Y. Zhang, X. Wei, L. Zhu, Bone homeostasis modulating orthopedic adhesive for the closed-loop management of osteoporotic fractures, *Small*. 2302704 (2023) 1–20, <https://doi.org/10.1002/smll.202302704>.
- [45] X. Ji, H. Shao, X. Li, M.W. Ullah, G. Luo, Z. Xu, L. Ma, X. He, Z. Lei, Q. Li, X. Jiang, G. Yang, Y. Zhang, Injectable immunomodulation-based porous chitosan microspheres/HPCH hydrogel composites as a controlled drug delivery system for osteochondral regeneration, *Biomaterials* 285 (2022) 121530, <https://doi.org/10.1016/j.biomaterials.2022.121530>.
- [46] S. Pan, Z. Yin, C. Shi, H. Xiu, G. Wu, Y. Heng, Z. Zhu, J. Zhang, J. Gui, Z. Yu, B. Liang, Multifunctional injectable hydrogel microparticles loaded with miR-29a abundant BMSCs derived exosomes enhanced bone regeneration by regulating osteogenesis and angiogenesis, *Small* 20 (2024) 1–19, <https://doi.org/10.1002/smll.202306721>.
- [47] L. Liu, Y. Xian, W. Wang, L. Huang, J. Fan, W. Ma, Y. Li, H. Liu, J.K. Yu, D. Wu, Meniscus-Inspired self-lubricating and friction-responsive hydrogels for protecting articular cartilage and improving exercise, *ACS Nano* 17 (2023) 24308–24319, <https://doi.org/10.1021/acsnano.3c10139>.
- [48] M. Chen, Y. Lu, Y. Liu, Q. Liu, S. Deng, Y. Liu, X. Cui, J. Liang, X. Zhang, Y. Fan, Q. Wang, Injectable microgels with hybrid exosomes of chondrocyte-targeted FGFR3 gene-editing and self-renewable lubrication for osteoarthritis therapy, *Adv. Mater.* 36 (2024) 1–20, <https://doi.org/10.1002/adma.202312559>.
- [49] Y. Yao, G. Wei, L. Deng, W. Cui, Visualizable and lubricating hydrogel microspheres via NanoPOSS for cartilage regeneration, *Adv. Sci.* 10 (2023) 1–13, <https://doi.org/10.1002/advs.202207438>.
- [50] Y. Lei, X. Wang, J. Liao, J. Shen, Y. Li, Z. Cai, N. Hu, X. Luo, W. Cui, W. Huang, Shear-responsive boundary-lubricated hydrogels attenuate osteoarthritis, *Bioact. Mater.* 16 (2022) 472–484, <https://doi.org/10.1016/j.bioactmat.2022.02.016>.
- [51] F. Liang, Y. Yang, Y. Chen, J. Xie, S. Liu, Z. Tan, L. Tian, Z. Yu, Z. Shi, P. Xie, H. Ding, Q. Yang, Ropivacaine microsphere-loaded electroconductive nerve dressings for long-acting analgesia and functional recovery following diabetic peripheral nerve injury, *Mater. Today Bio.* 21 (2023) 100712, <https://doi.org/10.1016/j.mtbio.2023.100712>.
- [52] M. Szustak, E. Gendaszewska-Darmach, Extracellular nucleotides selectively induce migration of chondrocytes and expression of type II collagen, *Int. J. Mol. Sci.* 21 (2020) 1–13, <https://doi.org/10.3390/ijms21155227>.
- [53] J. Magisetty, U.R. Pendurthi, C.T. Esmon, L. Vijaya Mohan Rao, EPCR deficiency or function-blocking antibody protects against joint bleeding-induced pathology in hemophilia mice, *Blood* 135 (2020) 2211–2223, <https://doi.org/10.1182/blood.2019003824>.
- [54] K.R. Sorensen, K. Roepstorff, B. Wiinberg, A.K. Hansen, M. Tranholm, L. N. Nielsen, M. Kjølgaard-Hansen, The F8–/– rat as a model of hemophilic arthropathy, *J. Thromb. Haemostasis* 14 (2016) 1216–1225, <https://doi.org/10.1111/jth.13328>.
- [55] J. Chen, J. Yang, L. Wang, X. Zhang, B.C. Heng, D.A. Wang, Z. Ge, Modified hyaluronic acid hydrogels with chemical groups that facilitate adhesion to host

- tissues enhance cartilage regeneration, *Bioact. Mater.* 6 (2021) 1689–1698, <https://doi.org/10.1016/j.bioactmat.2020.11.020>.
- [56] L. He, T. He, J. Xing, Q. Zhou, L. Fan, C. Liu, Y. Chen, D. Wu, Z. Tian, B. Liu, L. Rong, Bone marrow mesenchymal stem cell-derived exosomes protect cartilage damage and relieve knee osteoarthritis pain in a rat model of osteoarthritis, *Stem Cell Res. Ther.* 11 (2020) 1–15, <https://doi.org/10.1186/s13287-020-01781-w>.
- [57] K. Ma, T. Pham, J. Wang, I.S. O'Sullivan, A. DiCamillo, S. Du, F. Mwale, Z. Ferooqi, G. Votta-Velis, B. Bruce, A.J. van Wijnen, Y. Liu, H.J. Im, Nanoparticle-based inhibition of vascular endothelial growth factor receptors alleviates osteoarthritis pain and cartilage damage, *Sci. Adv.* 10 (2024) 1–17, <https://doi.org/10.1126/sciadv.adv5501>.
- [58] Y. Di Xu, X.C. Liang, Z.P. Li, Z.S. Wu, J. Yang, S.Z. Jia, R. Peng, Z.Y. Li, X. H. Wang, F.J. Luo, J.J. Chen, W.X. Cheng, P. Zhang, Z.G. Zha, R. Zeng, H. T. Zhang, Apoptotic body-inspired nanotherapeutics efficiently attenuate osteoarthritis by targeting BRD4-regulated synovial macrophage polarization, *Biomaterials* 306 (2024), <https://doi.org/10.1016/j.biomaterials.2024.122483>.
- [59] M. Ma, F. Zou, B. Abudurehman, F. Han, G. Xu, Y.J. Xie, K. Qiao, J. Peng, Y. Guan, H. Meng, Y. Zheng, Magnetic microcarriers with accurate localization and proliferation of mesenchymal stem cell for cartilage defects repairing, *ACS Nano* 17 (2023) 6373–6386, <https://doi.org/10.1021/acsnano.2c10995>.
- [60] K.A. Kimmerling, A.H. Gomoll, J. Farr, K.C. Mowry, Amniotic suspension allograft modulates inflammation in a rat pain model of osteoarthritis, *J. Orthop. Res.* 38 (2020) 1141–1149, <https://doi.org/10.1002/jor.24559>.
- [61] W. Fang, L. Yang, Y. Chen, Q. Hu, Bioinspired multifunctional injectable hydrogel for hemostasis and infected wound management, *Acta Biomater.* 161 (2023) 50–66, <https://doi.org/10.1016/j.actbio.2023.01.021>.
- [62] X. Li, H. Cheng, X. Huang, S. Li, R. Yang, J. Wang, X. Wang, Facile construction of chitin/graphene nanocomposite sponges for efficient hemostasis, *ACS Sustain. Chem. Eng.* 8 (2020) 18377–18385, <https://doi.org/10.1021/acscuschemeng.0c04721>.
- [63] S. Jin, Y. Wang, X. Wu, Z. Li, L. Zhu, Y. Niu, Y. Zhou, Y. Liu, Young exosome nanoparticles restore aging-impaired tendon stem/progenitor cell function and reparative capacity, *Adv. Mater.* 35 (2023) 1–17, <https://doi.org/10.1002/adma.202211602>.
- [64] C. Liu, L. Fan, M. Guan, Q. Zheng, J. Jin, X. Kang, Z. Gao, X. Deng, Y. Shen, G. Chu, J. Chen, Z. Yu, L. Zhou, Y. Wang, A redox homeostasis modulatory hydrogel with GLRX3+ extracellular vesicles attenuates disc degeneration by suppressing nucleus pulposus cell senescence, *ACS Nano* 17 (2023) 13441–13460, <https://doi.org/10.1021/acsnano.3c01713>.
- [65] Q. Li, H. Yu, M. Sun, P. Yang, X. Hu, Y. Ao, J. Cheng, The tissue origin effect of extracellular vesicles on cartilage and bone regeneration, *Acta Biomater.* 125 (2021) 253–266, <https://doi.org/10.1016/j.actbio.2021.02.039>.
- [66] J. Thomas, V. Chopra, S. Rajput, R. Guha, N. Chattopadhyay, D. Ghosh, Post-implantation stiffening by a bioinspired, double-network, self-healing hydrogel facilitates minimally invasive cell delivery for cartilage regeneration, *Biomacromolecules* 24 (2023) 3313–3326, <https://doi.org/10.1021/acs.biomac.3c00351>.
- [67] J. Liu, C. Tang, J. Huang, J. Gu, J. Yin, G. Xu, S. Yan, Nanofiber composite microchannel-containing injectable hydrogels for cartilage tissue regeneration, *Adv. Healthcare Mater.* 12 (2023) 1–14, <https://doi.org/10.1002/adhm.202302293>.
- [68] S.W. Kim, D.Y. Kim, H.H. Roh, H.S. Kim, J.W. Lee, K.Y. Lee, Three-dimensional bioprinting of cell-laden constructs using polysaccharide-based self-healing hydrogels, *Biomacromolecules* 20 (2019) 1860–1866, <https://doi.org/10.1021/acs.biomac.8b01589>.
- [69] T. Zhou, J. Ran, P. Xu, L. Shen, Y. He, J. Ye, L. Wu, C. Gao, A hyaluronic acid/platelet-rich plasma hydrogel containing MnO<sub>2</sub> nanozymes efficiently alleviates osteoarthritis in vivo, *Carbohydr. Polym.* 292 (2022) 119667, <https://doi.org/10.1016/j.carbpol.2022.119667>.
- [70] W. Hu, X. Yao, Y. Li, J. Li, J. Zhang, Z. Zou, F. Kang, S. Dong, Injectable hydrogel with selenium nanoparticles delivery for sustained glutathione peroxidase activation and enhanced osteoarthritis therapeutics, *Mater. Today Bio.* 23 (2023) 100864, <https://doi.org/10.1016/j.mtbio.2023.100864>.
- [71] E.C. Beck, M. Barragan, M.H. Tadros, S.H. Gehrke, M.S. Detamore, Approaching the compressive modulus of articular cartilage with a decellularized cartilage-based hydrogel, *Acta Biomater.* 38 (2016) 94–105, <https://doi.org/10.1016/j.actbio.2016.04.019>.
- [72] L.P. Yan, J. Silva-Correia, M.B. Oliveira, C. Vilela, H. Pereira, R.A. Sousa, J. F. Mano, A.L. Oliveira, J.M. Oliveira, R.L. Reis, Bilayered silk/silk-nanoCaP scaffolds for osteochondral tissue engineering: in vitro and in vivo assessment of biological performance, *Acta Biomater.* 12 (2015) 227–241, <https://doi.org/10.1016/j.actbio.2014.10.021>.
- [73] B.A.G. de Melo, Y.A. Jodas, S. Mehrotra, M.A. Calabrese, T. Kamperman, B. B. Mandal, M.H.A. Santana, E. Alsborg, J. Leijten, S.R. Shin, 3D printed cartilage-like tissue constructs with spatially controlled mechanical properties, *Adv. Funct. Mater.* 29 (2019), <https://doi.org/10.1002/adfm.201906330>.
- [74] Y. Wu, B. Ayan, K.K. Moncal, Y. Kang, A. Dhawan, S. V Koduru, D.J. Ravnicek, F. Kamal, I.T. Ozbolat, Hybrid bioprinting of zonally stratified human articular cartilage using scaffold-free tissue strands as building blocks, *Adv. Healthcare Mater.* 9 (2020) e2001657, <https://doi.org/10.1002/adhm.202001657>.
- [75] I.H. Yang, C.Y. Kuan, Z.Y. Chen, C.H. Li, C.Y. Chi, Y.Y. Lin, Y.J. Liang, W.T. Kuo, Y.A. Li, F.H. Lin, Engineered cell-laden thermosensitive poly(N-isopropylacrylamide)-immobilized gelatin microspheres as 3D cell carriers for regenerative medicine, *Mater. Today Bio.* 15 (2022), <https://doi.org/10.1016/j.mtbio.2022.100266>.
- [76] S. Gautam, C. Sharma, S.D. Purohit, H. Singh, A.K. Dinda, P.D. Potdar, C.F. Chou, N.C. Mishra, Gelatin-polycaprolactone-nanohydroxyapatite electrospun nanocomposite scaffold for bone tissue engineering, *Mater. Sci. Eng. C* 119 (2021) 111588, <https://doi.org/10.1016/j.msec.2020.111588>.
- [77] X. Wang, Q. Shen, C. Zhang, W. Jia, L. Han, Q. Yu, Chicken leg bone as a source of chondroitin sulfate, *Carbohydr. Polym.* 207 (2019) 191–199, <https://doi.org/10.1016/j.carbpol.2018.11.086>.
- [78] G. Wu, F. Ma, Y. Xue, Y. Peng, L. Hu, X. Kang, Q. Sun, D.F. Ouyang, B. Tang, L. Lin, Chondroitin sulfate zinc with antibacterial properties and anti-inflammatory effects for skin wound healing, *Carbohydr. Polym.* 278 (2022) 118996, <https://doi.org/10.1016/j.carbpol.2021.118996>.
- [79] J. Cao, G. He, X. Ning, C. Wang, L. Fan, Y. Yin, W. Cai, Hydroxypropyl chitosan-based dual self-healing hydrogel for adsorption of chromium ions, *Int. J. Biol. Macromol.* 174 (2021) 89–100, <https://doi.org/10.1016/j.ijbiomac.2021.01.089>.
- [80] Y. Luo, L. Fan, C. Liu, H. Wen, S. Wang, P. Guan, D. Chen, C. Ning, L. Zhou, G. Tan, An injectable, self-healing, electroconductive extracellular matrix-based hydrogel for enhancing tissue repair after traumatic spinal cord injury, *Bioact. Mater.* 7 (2022) 98–111, <https://doi.org/10.1016/j.bioactmat.2021.05.039>.
- [81] X. Yan, A.A. Wardana, L.P. Wigati, F. Meng, S. Leonard, F.N. Nkede, F. Tanaka, F. Tanaka, Characterization and bio-functional performance of chitosan/poly(vinyl alcohol)/trans-cinnamaldehyde ternary biopolymeric films, *Int. J. Biol. Macromol.* 246 (2023) 125680, <https://doi.org/10.1016/j.ijbiomac.2023.125680>.
- [82] D. Trucco, L. Vannozzi, E. Teblum, M. Telkhozayeva, G.D. Nessim, S. Affatato, H. Al-Haddad, G. Lisignoli, L. Ricotti, Graphene oxide-doped gellan gum-PEGDA bilayered hydrogel mimicking the mechanical and lubrication properties of articular cartilage, *Adv. Healthcare Mater.* 10 (2021), <https://doi.org/10.1002/adhm.202001434>.
- [83] F. Yang, J. Zhao, W.J. Koshut, J. Watt, J.C. Riboh, K. Gall, B.J. Wiley, A synthetic hydrogel composite with the mechanical behavior and durability of cartilage, *Adv. Funct. Mater.* 30 (2020) 1–8, <https://doi.org/10.1002/adfm.202003451>.
- [84] C. Luo, A. Guo, Y. Zhao, X. Sun, A high strength, low friction, and biocompatible hydrogel from PVA, chitosan and sodium alginate for articular cartilage, *Carbohydr. Polym.* 286 (2022) 119268, <https://doi.org/10.1016/j.carbpol.2022.119268>.
- [85] G. Yang, Y. Li, S. Zhang, Y. Wang, L. Yang, Q. Wan, X. Pei, J. Chen, X. Zhang, J. Wang, Double-cross-linked hydrogel with long-lasting underwater adhesion: enhancement of maxillofacial in situ and onlay bone retention, *ACS Appl. Mater. Interfaces* 15 (2023) 46639–46654, <https://doi.org/10.1021/acsmi.3c09117>.
- [86] Y. Hao, W. Zhao, H. Zhang, W. Zheng, Q. Zhou, Carboxymethyl chitosan-based hydrogels containing fibroblast growth factors for triggering diabetic wound healing, *Carbohydr. Polym.* 287 (2022) 119336, <https://doi.org/10.1016/j.carbpol.2022.119336>.
- [87] H. Wang, M. Wang, J. Wu, S. Zhu, Y. Ye, Y. Liu, K. Li, R. Li, Y. Zhang, M. Wei, X. Yang, L. Meng, Nature-Inspired gelatin-based adhesive hydrogel: a rapid and user-friendly solution for hemostatic applications, *Adv. Healthcare Mater.* (2024) e2304444, <https://doi.org/10.1002/adhm.202304444>.
- [88] Q. Ling, W. Liu, J. Liu, L. Zhao, Z. Ren, H. Gu, Highly sensitive and robust polysaccharide-based composite hydrogel sensor integrated with underwater repeatable self-adhesion and rapid self-healing for human motion detection, <https://doi.org/10.1021/acsmi.2c01785>, 2022.
- [89] X. Lei, C. Zou, J. Hu, M. Fan, Y. Jiang, M. Xiong, C. Han, X. Zhang, Y. Li, L. Zhao, R. Nie, J. Li-ling, A Self-Assembly Pro-coagulant Powder Capable of Rapid Gelling Transformation and Wet Adhesion for the Efficient Control of Non-compressible Hemorrhage, vol. 2306289, 2024, pp. 1–17, <https://doi.org/10.1002/advs.202306289>.
- [90] Z. Li, Y. Zhao, X. Ouyang, Y. Yang, Y. Chen, Q. Luo, Y. Zhang, D. Zhu, X. Yu, L. Li, Biomimetic hybrid hydrogel for hemostasis, adhesion prevention and promoting regeneration after partial liver resection, *Bioact. Mater.* 11 (2022) 41–51, <https://doi.org/10.1016/j.bioactmat.2021.10.001>.
- [91] X. Wang, Y. Guo, J. Li, M. You, Y. Yu, J. Yang, G. Qin, Q. Chen, Tough wet adhesion of hydrogen-bond-based hydrogel with on-demand debonding and efficient hemostasis, *ACS Appl. Mater. Interfaces* 14 (2022) 36166–36177, <https://doi.org/10.1021/acsmi.2c10202>.
- [92] S. Guo, Y. Ren, R. Chang, Y. He, D. Zhang, F. Guan, M. Yao, Injectable self-healing adhesive chitosan hydrogel with antioxidant, antibacterial, and hemostatic activities for rapid hemostasis and skin wound healing, <https://doi.org/10.1021/acsmi.2c08870>, 2022.
- [93] A.E. Pulles, S.C. Mastbergen, R.E.G. Schutgens, F.P.J.G. Lafeber, L.F.D. van Vulpen, Pathophysiology of hemophilic arthropathy and potential targets for therapy, *Pharmacol. Res.* 115 (2017) 192–199, <https://doi.org/10.1016/j.phrs.2016.11.032>.
- [94] K.R. Christensen, M. Kjelgaard-Hansen, L.N. Nielsen, B. Wiinberg, F.A. Althoehn, N.B. Poulsen, K.K. Vols, A.P. Thyme, K.M. Lövgren, A. Kornerup Hansen, K. Roepstorff, Rapid inflammation and early degeneration of bone and cartilage revealed in a time-course study of induced haemarthrosis in haemophilic rats, *Rheumatol. (United Kingdom)*. 58 (2019) 588–599, <https://doi.org/10.1093/rheumatology/key186>.
- [95] E.J. Cooke, J.Y. Zhou, T. Wyseure, S. Joshi, V. Bhat, D.L. Durden, L.O. Mosnier, A. von Drygalski, Vascular permeability and remodelling coincide with inflammatory and reparative processes after joint bleeding in factor VIII-deficient mice, *Thromb. Haemost.* 118 (2018) 1036–1047, <https://doi.org/10.1055/s-0038-1641755>.
- [96] E.J. Cooke, B.C. Joseph, C.A. Nasamran, K.M. Fisch, A. von Drygalski, Maladaptive lymphangiogenesis is associated with synovial iron accumulation and delayed clearance in factor VIII-deficient mice after induced hemarthrosis,

- J. Thromb. Haemostasis 21 (2023) 2390–2404, <https://doi.org/10.1016/j.jtha.2023.04.022>.
- [97] J. Magisetty, V. Kondreddy, S. Keshava, K. Das, C.T. Esmon, U.R. Pendurthi, L.V. M. Rao, Selective inhibition of activated protein C anticoagulant activity protects against hemophilic arthropathy in mice, *Blood* 139 (2022) 2830–2841, <https://doi.org/10.1182/blood.2021013119>.
- [98] L. Fan, P. Guan, C. Xiao, H. Wen, Q. Wang, C. Liu, Y. Luo, L. Ma, G. Tan, P. Yu, L. Zhou, C. Ning, Exosome-functionalized polyetheretherketone-based implant with immunomodulatory property for enhancing osseointegration, *Bioact. Mater.* 6 (2021) 2754–2766, <https://doi.org/10.1016/j.bioactmat.2021.02.005>.
- [99] W. Jiang, X. Xiang, M. Song, J. Shen, Z. Shi, W. Huang, H. Liu, An all-silk-derived bilayer hydrogel for osteochondral tissue engineering, *Mater. Today Bio.* 17 (2022) 100485, <https://doi.org/10.1016/j.mtbio.2022.100485>.
- [100] Y. Yan, L.B. Zhang, R. Ma, M.N. Wang, J. He, P.P. Wang, Q.W. Tao, Y. Xu, Jolkinolide B ameliorates rheumatoid arthritis by regulating the JAK2/STAT3 signaling pathway, *Phytomedicine* 124 (2024), <https://doi.org/10.1016/j.phymed.2023.155311>.
- [101] Y. Peng, Y. Li, Y. Pi, X. Yue, Effects of almond (*Armeniaca Sibirica* L. Lam) polysaccharides on gut microbiota and anti-inflammatory effects on LPS-induced RAW264.7 cells, *Int. J. Biol. Macromol.* 263 (2024) 130098, <https://doi.org/10.1016/j.ijbiomac.2024.130098>.
- [102] A.T. Kim, D.O. Kim, Anti-inflammatory effects of vanadium-binding protein from *Halocynthia roretzi* in LPS-stimulated RAW264.7 macrophages through NF- $\kappa$ B and MAPK pathways, *Int. J. Biol. Macromol.* 133 (2019) 732–738, <https://doi.org/10.1016/j.ijbiomac.2019.04.106>.
- [103] J. Chen, D.L. Li, L.N. Xie, Y. ran Ma, P.P. Wu, C. Li, W.F. Liu, K. Zhang, R.P. Zhou, X.T. Xu, X. Zheng, X. Liu, Synergistic anti-inflammatory effects of silibinin and thymol combination on LPS-induced RAW264.7 cells by inhibition of NF- $\kappa$ B and MAPK activation, *Phytomedicine* 78 (2020) 153309, <https://doi.org/10.1016/j.phymed.2020.153309>.
- [104] Q. Zhao, W. Zheng, Z. Yuan, X. Wang, A. Huang, Anti-inflammatory effect of two novel peptides derived from Binglangjiang buffalo whey protein in lipopolysaccharide-stimulated RAW264.7 macrophages, *Food Chem.* 429 (2023) 136804, <https://doi.org/10.1016/j.foodchem.2023.136804>.
- [105] M. Dai, B. Sui, Y. Xue, X. Liu, J. Sun, Cartilage repair in degenerative osteoarthritis mediated by squid type II collagen via immunomodulating activation of M2 macrophages, inhibiting apoptosis and hypertrophy of chondrocytes, *Biomaterials* 180 (2018) 91–103, <https://doi.org/10.1016/j.biomaterials.2018.07.011>.
- [106] S. Chen, W. Chen, Y. Chen, X. Mo, C. Fan, Chondroitin sulfate modified 3D porous electrospun nanofiber scaffolds promote cartilage regeneration, *Mater. Sci. Eng., C* 118 (2021) 111312, <https://doi.org/10.1016/j.msec.2020.111312>.
- [107] S. Zhang, K.Y.W. Teo, S.J. Chuah, R.C. Lai, S.K. Lim, W.S. Toh, MSC exosomes alleviate temporomandibular joint osteoarthritis by attenuating inflammation and restoring matrix homeostasis, *Biomaterials* 200 (2019) 35–47, <https://doi.org/10.1016/j.biomaterials.2019.02.006>.
- [108] S. Wang, B. Luo, B. Bai, Q. Wang, H. Chen, X. Tan, Z. Tang, S. Shen, H. Zhou, Z. You, G. Zhou, D. Lei, 3D printed chondrogenic functionalized PGS bioactive scaffold for cartilage regeneration, *Adv. Healthcare Mater.* 12 (2023) 1–15, <https://doi.org/10.1002/adhm.202301006>.
- [109] Q. Chen, Y. Jin, T. Chen, H. Zhou, X. Wang, O. Wu, L. Chen, Z. Zhang, Z. Guo, J. Sun, A. Wu, Q. Qian, Materials Today Bio Injectable nanocomposite hydrogels with enhanced lubrication and antioxidant properties for the treatment of osteoarthritis, *Mater. Today Bio.* 25 (2024) 100993, <https://doi.org/10.1016/j.mtbio.2024.100993>.
- [110] M.K. Satapathy, Y.B. Manga, K.K. Ostrikov, W. Chiang, A. Pandey, R. Lekha, B. Nyambat, E. Chuang, C. Chen, Microplasma cross-linked graphene oxide-gelatin hydrogel for cartilage reconstructive surgery, <https://doi.org/10.1021/acsami.9b14073>, 2020.
- [111] C. Gong, J. Wang, F. Tang, D. Tong, Z. Wang, Z. Zhou, R. Ruan, J. Zhang, J. Song, H. Yang, Bionic bilayer scaffold for synchronous hyperthermia therapy of orthotopic osteosarcoma and osteochondral regeneration, <https://doi.org/10.1021/acsami.3c18171>, 2024.
- [112] P. Wojdasiewicz, Ł.A. Poniatowski, P. Nauman, T. Mandat, A. Paradowska-Gorycka, K. Romanowska-Próchnicka, D. Szukiewicz, A. Kotela, Ł. Kubaszewski, I. Kotela, I. Kurkowska-Jastrzębska, R. Gasik, Cytokines in the pathogenesis of hemophilic arthropathy, *Cytokine Growth Factor Rev.* 39 (2018) 71–91, <https://doi.org/10.1016/j.cytogfr.2017.11.003>.